VĚDECKÉ SPISY VYSOKÉHO UČENÍ TECHNICKÉHO V BRNĚ

*Edice Habilitační a inaugurační spisy, sv. 532*

*ISSN 1213-418X*

**Pavel Charvát**

# LATENT HEAT THERMAL ENERGY STORAGE IN SOLAR AIR HEATING

VYSOKÉ UČENÍ TECHNICKÉ V BRNĚ
Fakulta strojního inženýrství
Energetický ústav

**Ing. Pavel Charvát, Ph.D.**

# LATENT HEAT THERMAL ENERGY STORAGE IN SOLAR AIR HEATING

# AKUMULACE TEPLA S VYUŽITÍM ZMĚNY SKUPENSTVÍ PŘI SOLÁRNÍM OHŘEVU VZDUCHU

Zkrácená verze habilitační práce
v oboru Konstrukční a procesní inženýrství

VUTIUM

BRNO 2016

**KEYWORDS**
Latent heat thermal energy storage, phase change materials, solar air heating.

**KLÍČOVÁ SLOVA**
Akumulace tepla při změně skupenství, materiály se změnou skupenství, solární ohřev vzduchu.

**MÍSTO ULOŽENÍ PRÁCE**

Energetický ústav
Fakulta strojního inženýrství
Vysoké učení technické v Brně
Technická 2896/2
616 69 Brno


ISBN 978-80-214-5324-1
ISSN 1213-418X

## ABOUT THE AUTHOR

Pavel Charvát, born October 27, 1971, received a master's degree in Aircraft design from Brno University of Technology in 1995 and a Ph.D. from the same university in 2003. His Ph.D. thesis dealt with the interferometric investigation of non-isothermal air jets. Pavel Charvat is currently an assistant professor at the Department of Thermodynamics and Environmental Engineering at the Faculty of Mechanical Engineering of Brno University of Technology. His main areas of interest are building ventilation, solar thermal energy, and latent heat thermal energy storage.

Pavel Charvát has been involved in the investigations of solar air heating since 2000 when he joined the research team of the project *Performance, Efficiency, and Optimization of Ventilating Systems in Solar Buildings* (a project within the framework of the COST action G3: Industrial Ventilation). A year later he became the principal investigator of another project in the same COST action *(Solar Radiation Induced Convection In Highly Glazed Spaces)*. Both projects were completed in 2003.

After receiving his Ph.D., Pavel Charvát became the principal investigator of the post-doctoral project *Residential Hybrid Ventilation Assisted with Solar Chimneys* (2004-2006, funded by the Czech Science Foundation). He started to conduct research in the area of latent heat thermal energy storage in 2007 when he became the principle investigator of the project *Solar chimneys and phase change materials in passive cooling of buildings* (2007-2009, Czech Science Foundation). Latent heat thermal energy storage has been the main research interest of Pavel Charvát in the last several years as he was the principle investigator of two other projects in this area; *Phase change materials for increased energy efficiency of air-based solar thermal systems in buildings* (2010-2012, COST Action TU0802: Next generation cost effective phase change materials for increased energy efficiency in renewable energy systems in buildings) and *The attenuation of fluid temperature oscillations using latent heat thermal storage* (2011-2013, Czech Science Foundation). As a research team member, Pavel Charvát has participated in several other projects including two EU framework program projects.

Pavel Charvát co-authored 9 papers published in indexed journals and over 70 conference papers and contributions to technical journals. He has peer reviewed papers for several indexed journals (e.g. Energy and Buildings, Solar Energy, Journal of Building Performance Simulation).

Pavel Charvát is currently teaching two courses (*Environmental engineering* and *Energy simulations)* in the master's degree program Environmental Engineering. He used to teach tutorials in the undergraduate *Thermodynamics* course and the laboratory classes in *Experimental methods* course. Pavel Charvat has supervised 19 bachelor's thesis, 23 master's theses and he was an advisor-specialist of one Ph.D. student.

Pavel Charvát is a member of the International Building Performance Simulation Association (IBPSA), the Czech Society of Environmental Engineering, and the Technical Standard Committee TNK 75 "Ventilation technology" (an advisory board of the Czech Office for Standards, Metrology and Testing).

# 1 INTRODUCTION

Solar radiation is the most abundant source of renewable energy available to mankind. The total amount of solar radiation incident on the surface of the Earth many times exceeds the energy needs of today's society. Even the solar radiation incident on land far exceeds the world total energy consumption. Solar radiation is thus a very promising source of renewable energy. For practical utilization the solar radiation needs to be converted either to heat (in case of solar thermal applications) or to electricity (in case of solar photovoltaic applications).

The main disadvantage of solar radiation as a source of energy is its non-even distribution in time. The intensity of solar radiation at one geographic location changes significantly during a day and throughout the year. For that reason, most of the systems utilizing solar radiation cannot effectively operate without some form of energy storage. The necessity of energy storage is the main roadblock for further expansion of renewable energy sources in general and solar energy in particular. The solar thermal systems have certain advantages over the photovoltaic systems in terms of energy storage as heat is much easier to store than other forms of energy. Even then, heat storage represents an extra cost that increases the overall costs of solar energy systems.

Most solar thermal systems are utilized in low-temperature applications such as solar space heating, solar drying, and solar domestic hot water heating (SDHW). The heat transfer fluids (HTFs) in such solar thermal applications usually have a temperature of less than 100 °C. Therefore, water can readily be used as both the heat transfer fluid and the heat storage medium in such cases. The solar thermal systems producing heat for technological processes or power generation quite often operate at temperatures far exceeding 100 °C, where water is no longer suitable as a HTF or as a heat storage medium. The highest operating temperatures are achieved in concentrated solar thermal power plants where the heliostats or the parabolic mirror troughs are used to concentrate solar radiation. The efficiency of a thermodynamic cycle increases with the increasing temperature of the heat source (thermal reservoir) and thus it is desirable to achieve as high temperature of the hot reservoir as technically feasible. At the Ivanpah Solar Electric Generating System that was recently built in Mojave desert, CA, USA, and where heliostats are used to concentrate solar radiation, the receiver output temperature exceeds 560 °C. The annual solar-to-electricity efficiency of 28.72% of the Ivanpah solar thermal power plant is higher than the conversion efficiency of the solar cells currently used in the photovoltaic power plants.

This habilitation thesis deals with latent heat thermal energy storage (LHTES) in solar air heating. Air has a very low thermal capacity per unit of volume and for that reason it cannot be used as a heat storage medium even when it is used as a HTF. On the other hand, the advantage of air as a HTF is its availability and the fact that it can be used in a wide range of temperatures. Though air is in some cases used as a HTF in concentrated solar thermal plants this thesis focuses on the low-temperature solar air heating applications such as solar space heating, solar ventilation air heating or solar drying. Solar air heating can be supplemented with different ways of thermal energy storage in order to deal with the unsteady character of solar radiation. The sensible heat storage materials such as rocks, pebbles, concrete or bricks have commonly been used for thermal storage in solar air heating. These materials are non-expensive and have a long lifespan but their energy storage density is relatively small; particularly when thermal energy storage takes place in a narrow temperature interval. On the other hand, the release and absorption of latent heat when a material undergoes a phase change provides much larger heat storage capacity (and thus energy storage density) in a relatively small interval around the phase change temperature. The investigations reported in this thesis focused on two cases of latent heat thermal energy storage in solar air heating. The first case is the integration of a PCM with the solar absorber plate of an air solar collector. The second case is a PCM-air heat storage unit.

## 2 THERMAL ENERGY STORAGE

Energy has different forms and it is possible to change (convert) one form of energy into another. A modern society exploits many types of energy sources that produce various forms of energy. Several energy conversions usually take place between the primary energy source and the point of final energy consumption. As there is quite often a mismatch between the energy supply and the energy demand some form of energy storage needs to be used to bring supply and demand into balance. One form of energy is very often converted into another form of energy during the energy storage process and the opposite conversion takes place when the energy is released from energy storage. Actually, several conversions of one form of energy into another can take place during the energy storage cycle.

The final use of energy is quite often in the form of thermal energy (heat). Other forms of energy (chemical, electrical, etc.) are often converted to heat just before the final use (space heating, hot water heating, product drying, etc.). This is the area where thermal energy storage (TES) can be employed. Thermal energy storage is part of many thermal energy systems today. Heat, as the lowest form of energy, is relatively easy to store. The use of heat storage dates back thousands of years. Since prehistoric times people heated-up stones in the fire and then used them for various heating purposes. Cold storage is another area of thermal storage that dates back quite a long time. Cold storage is a kind of cold reservoir and thus it works in the opposite way to heat storage. The need to preserve food and beverages during their long-term storage brought about natural ice harvesting which is not only an example of cold storage but also an example of the utilization of latent heat in cold storage. Cold storage with natural ice and snow harvested in winter was used even in the first half of the 20th century when mechanical refrigeration was already widely available. Even today ice storage remains a common way of cold storage in many cooling systems with natural ice harvesting replaced by modern ice making technologies [1]. There are several thermal storage methods that differ in their principle, the energy storage density, storage temperature and other characteristics. The basic division of TES is shown in Fig. 1.

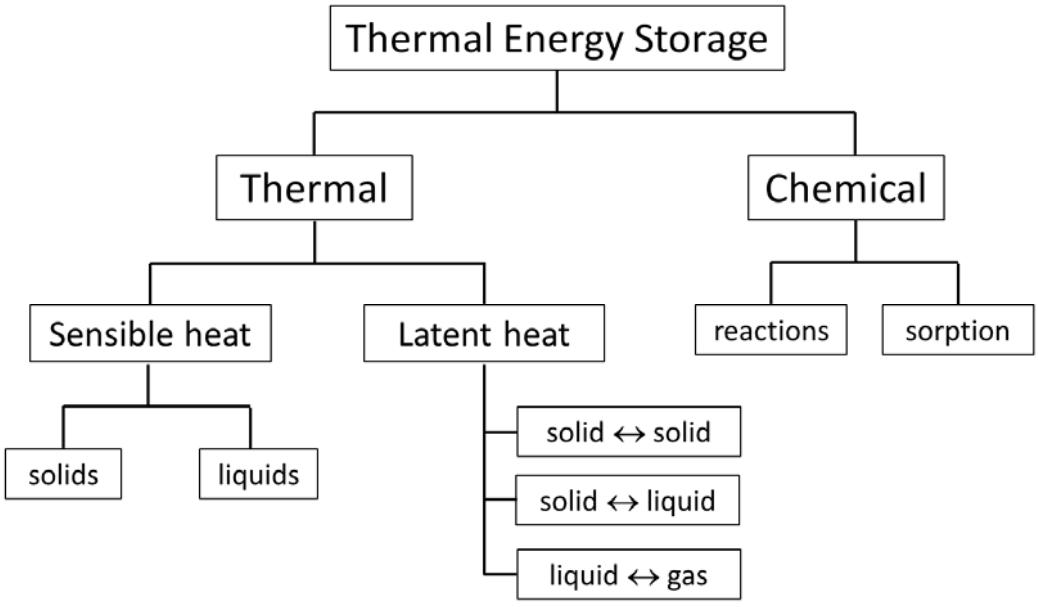


***Fig. 1*** *Thermal energy storage*

Matter can exist in three phases – solid, liquid, and gas – and the transition from one phase to another is associated with transfer of latent heat. The phase change is more or less an isothermal process; more for pure elements, less for the complex chemical substances and their mixtures.

Unlike sensible heat storage, where the amount of stored heat is proportional to the change in the temperature of the heat storage medium, latent heat storage theoretically allows to store heat at constant temperature. In practice it is a narrow temperature interval around the melting temperature of the heat storage material. The schematic representation of the isothermal phase changes during heating of matter can be seen in Fig. 2.

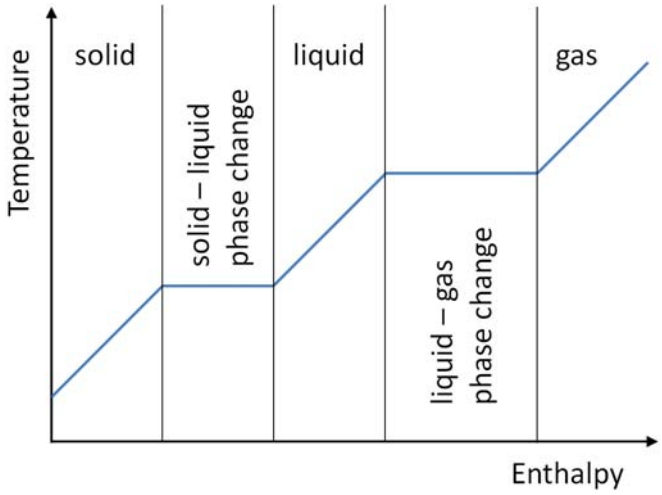


***Fig. 2*** *Phase changes of matter*

Though both the solid-liquid and the liquid-gas phase changes can be employed for latent heat storage, it is the solid-liquid phase change that is used in almost all the latent heat thermal energy storage systems [2], [3]. It would be theoretically possible to exploit the phase changes in the same state of the matter, such as the changes of the crystal structure in the solid state, but such phase changes are not used for thermal energy storage purposes in practice.

The amount of heat stored in latent heat storage between temperatures $T_1$ and $T_2$ when the melting temperature of the thermal storage material $T_{pch}$ is between $T_1$ and $T_2$ ($T_1 < T_{pch} < T_2$) can be expressed as

$$Q = m \int_{T_1}^{T_{pch}} c_{ps}\, dT + m\, H_m + m \int_{T_{pch}}^{T_2} c_{pl}\, dT \qquad (1)$$

where $m$ is the mass of heat storage medium, $c_{ps}$ is specific heat in the solid state, $H_m$ is the specific enthalpy of fusion and $c_{pl}$ is the specific heat in the liquid state. Eq. (1) is for an isothermal phase change that is more or less a textbook example. Most of the latent heat storage materials melt and solidify within a certain temperature range; therefore, the phase change in such cases is not isothermal.

## 2.1 ENERGY STORAGE DENSITY

The energy storage density is the amount of energy that can be stored in a certain volume or mass of energy storage material. In case of thermal energy storage the energy in question is thermal energy (heat) and thus we can speak about the heat storage density. The energy storage density is one of the most important factors in the practical design of energy storage systems. The higher the energy storage density the less space (volume) is needed for energy storage. When speaking about the energy storage density only the volume of the energy storage material is usually considered. Some heat storage technologies can be relatively complex, as in case of

thermochemical storage, and the necessary space for the installation of the technological components can significantly dilute the overall energy storage density. Different thermal energy storage methods provide different energy storage densities. On top of that, different energy storage media within one thermal energy storage method offer different energy storage densities. A comparison of energy storage densities for various thermal energy storage methods was presented by Hadron [4].

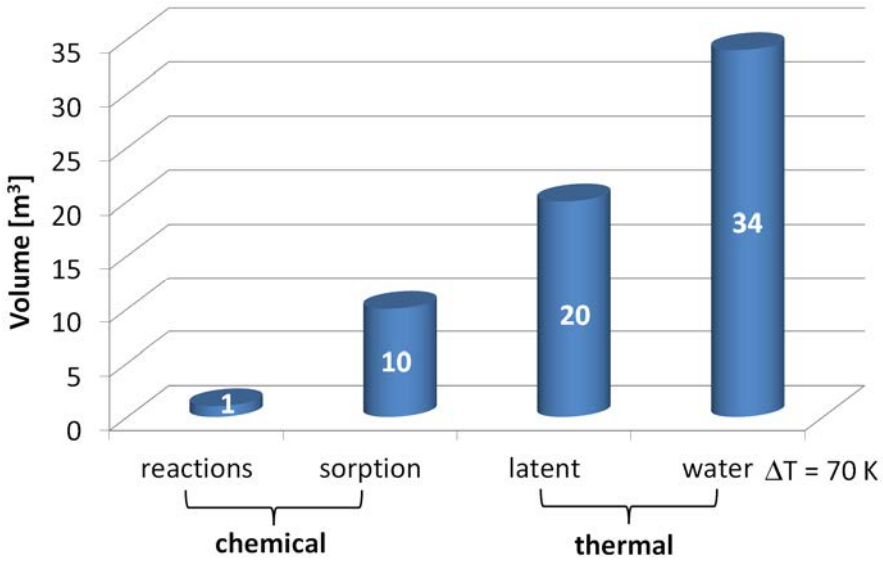


***Fig. 3*** *Volume needed to store 10 GJ of thermal energy*
*Figure created by author from data in [4]*

As can be seen in Fig. 3 the chemical reactions provide the highest energy storage density. However, the energy storage density is not the only factor that influences the amount of space needed for thermal energy storage. Water-based thermal energy storage does not require much technology beside a circulation pump and possibly a heat exchanger while the technology for chemical thermal energy storage can be quite complex. Also, the need for maintenance and the associated costs play an important role in decision making about a suitable thermal energy storage method. Many types of water-based sensible heat storage systems are used in homes all around the world at the moment, but it is hard to imagine that the thermochemical heat storage systems could be used in the same manner in the near future.

## 2.2 PHASE CHANGE MATERIALS

A large number of materials are known that melt at temperatures suitable for thermal energy storage (space heating and cooling, domestic hot water heating, etc.). However, beside the suitable melting temperature and heat of fusion these materials need to have certain thermodynamic and chemical properties to be usable as latent heat storage materials [5]. The materials for latent heat thermal energy storage are commonly called Phase Change Materials (with the abbreviation ‘PCM’ in the singular form and ‘PCMs’ in the plural form).

The phase change materials have become a well-established category in the material science and a significant afford is spent on the development of new PCMs with the specific sets of properties. A number of papers dealing with the phase change materials and their use in various technical applications have been published in recent years [6], [7], [8]. The PCMs can be divided into three basic categories as can be seen in Fig. 4.

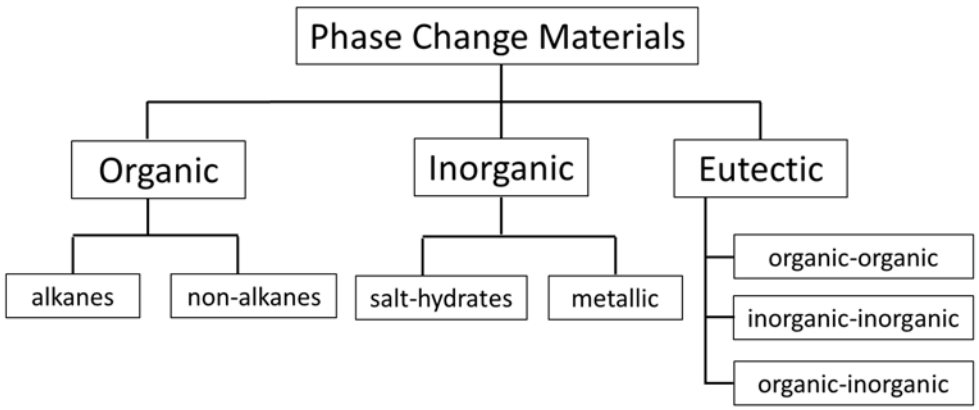


***Fig. 4*** *Classification of PCMs*

## 2.3 COMPACT STORAGE MODULES

Since the PCMs repeatedly change their state from solid to liquid during the heat storage cycles they need to be kept in some kind of containers or matrices. The ways in which the PCMs are contained depend on the TES application. In case of building-integrated latent heat storage the PCMs can sometimes be contained in a porous matrix such as stone, wood, concrete or other porous building material. The main disadvantage of this way of containment is that it is difficult to hold a PCM in the matrix when the PCM is in the liquid state. Another way of containment is the so called microencapsulation where a PCM is contained in microcapsules made of various materials. The diameter of the microcapsules is usually only a few micrometers (1 μm to 5 μm) but the capsules can even have diameters smaller than 1 μm [9]. The advantage of this way of containment is that the microencapsulated PCMs can be mixed with other materials (e.g. concrete or gypsum plaster). The disadvantage of the microencapsulation is the low thermal conductivity of most materials used for microcapsules. Another disadvantage is a relatively small mass-fraction of a PCM resulting into small total heat storage capacity. That is especially a problem when the microencapsulated PCM are mixed with other materials like concrete or plaster because the fraction of microencapsulated PCM is limited by the requirements on mechanical properties of the material [10].

Compact Storage Modules (CSMs) represent a specific way of macro-capsulation of the PCMs. The CSMs have different shapes and they can contain different amounts of PCMs. The CSMs can be filled with various types of PCMs. The CSMs are hermetically sealed; therefore, the handlers do not get in direct contact with the PCM during manipulation with CSMs. That makes the assembly of a LHTES unit relatively easy. The CSM panels produced by Rubitherm Technologies GmbH [11] were used in the investigations presented in this thesis. The Rubitherm CSM panels are aluminum containers that can accommodate various phase change materials. The length of the panels is 450 mm, width 300 mm and the thickness is 10 mm, 15 mm, or 20 mm. Different thicknesses mean different amount of PCM that can be accommodated in the CSM panel and also the different surface area to volume ratio. Since all investigations were done with air as a HTF the 10 mm thick CSM panels were used as they have the largest surface area to volume ratio.

**Fig. 5** CSM panel

# 3 AIR SOLAR COLLECTOR WITH LATENT HEAT STORAGE

An air solar collector is the main part of most solar air heating system. The air solar collectors are not as common as the collectors with liquid heat transfer fluids. The air solar collectors are often called solar air heaters. There are many designs of air solar collectors and thus several ways of their classification exist. One way of collector classification is according to the airflow path around the solar absorber plate. The four basic configurations are: a front-pass collector, a back-pass collector, a front-and-back pass collector and a through-pass collector (Fig. 6)

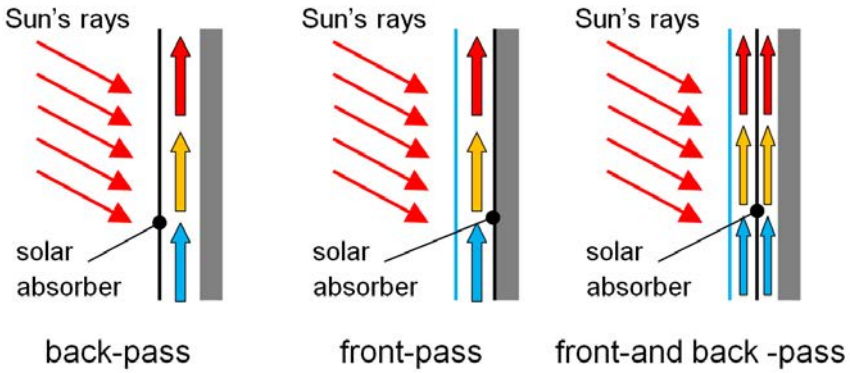


***Fig. 6*** *Configurations of air solar collectors*

The investigations into air solar collectors reported in this thesis focused on the influence of latent heat thermal energy storage, integrated with the solar absorber plate, on the collector behavior. Two experimental air solar collectors were built for this purpose. The collectors were of the front-and-back pass design as it provides larger heat exchange area than the front-pass or the back-pass design. The overall dimensions of the collectors can be seen in Fig. 7. One of the collectors had the solar absorber plate made of sheet metal. This design is referred to as the "light-weight collector" in the thesis. The solar absorber plate of the other collector consisted of 9 CSM panels filled with RT42 paraffin-based PCM. That design is referred to as the "collector with PCM." The transparent covers of the collectors were made of polymethyl methacrylate (PMMA).

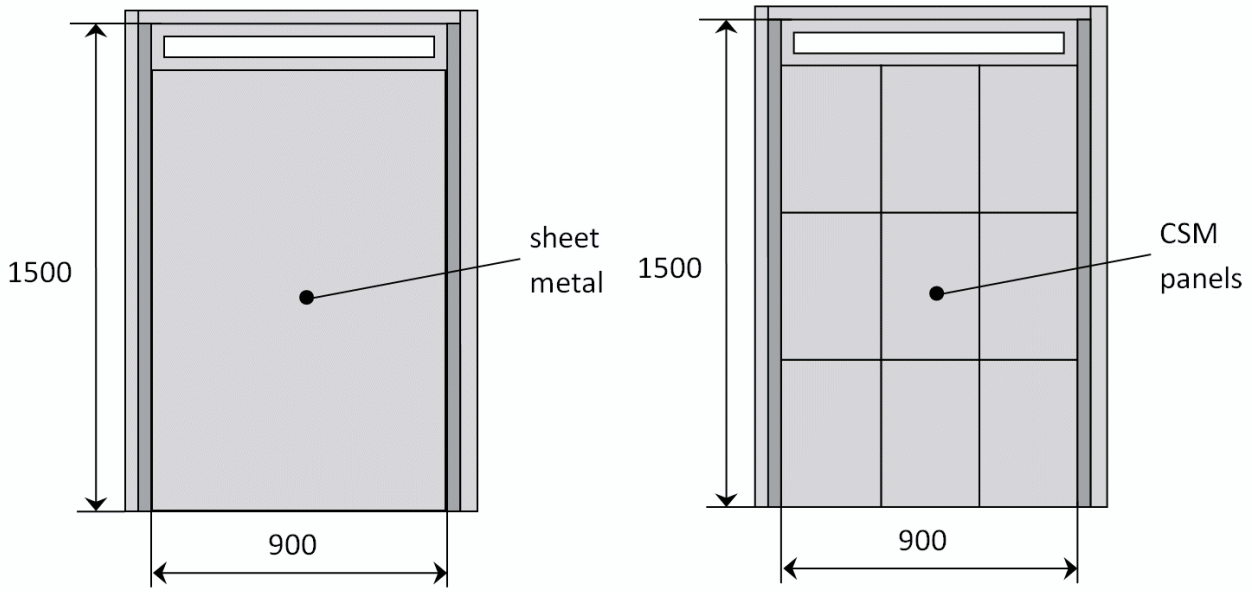


***Fig. 7*** *Dimensions of the experimental air solar collectors*

The PMMA has slightly worse optical properties than glass (especially the special glass for the collector covers), but it was much more practical for the experimental collectors. The goal was not to build high-performance air solar collectors but to build collectors that would be as similar to each other as possible. The collectors should only differ in the properties of the solar absorber plates. The same opaque black paint was applied on both solar absorber plates. The emissivity of the black-painted surfaces was not measured. The researchers, who carried out a study into the thermal performance of an air solar collector with the absorber plate made of recyclable aluminum cans, reported in their paper [12] the absorptance of a common black paint of 0.903 with the reflectance of 0.097. However, the authors refer to these values simply as optical properties and it is not clear whether the measured absorptance applies only to the visible light or to the entire spectrum of solar radiation. The idea behind having two identical air solar collectors (solar air heaters) was to conduct comparative measurements. The two collectors could be positioned side by side with the same slope and the same azimuth and thus exposed to the same incident radiation and other ambient conditions at the same time.

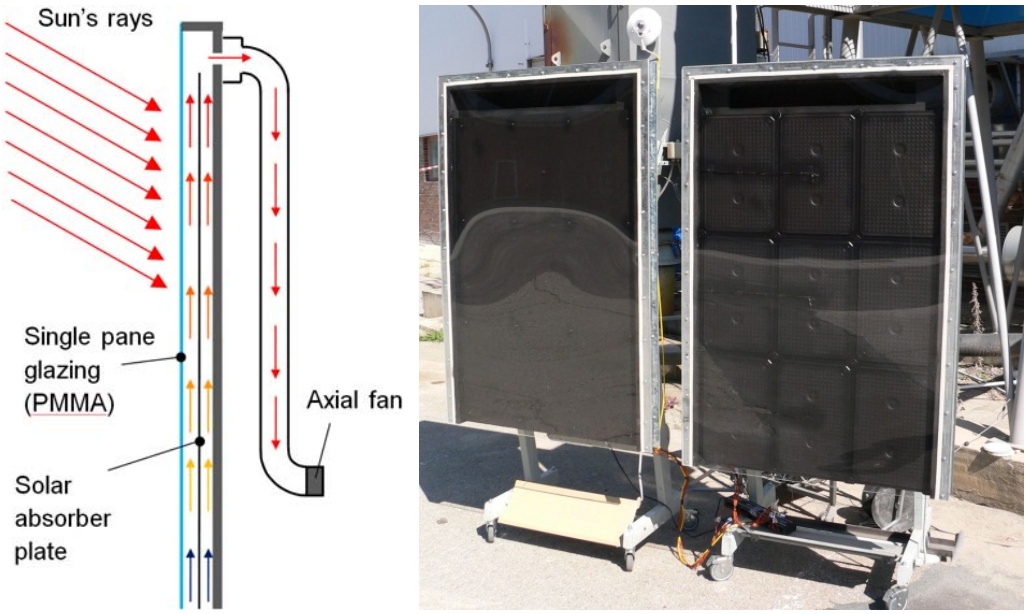


***Fig. 8*** *Experimental air solar collectors*

The ambient air entered the collectors at the bottom and it was drawn through the air cavities by axial fans located at the outlet (Fig. 8). The speed of the fans could be controlled and thus the desired air flow rate through the collectors could be achieved.

A number of sensors were used to monitor the ambient conditions as well as the performance of the collectors. A pyranometer was used to acquire the total solar radiation intensity incident on the surface of the collectors. A wind gauge was used to obtain wind speed and direction in the outdoor experiments but it was removed for the climatic chamber experiments. The air flow rate through the collectors was acquired by means of anemometric probes installed in the round ducts on the backside of the collectors. The air temperature and the temperature of the solar absorber plates were measured at several locations in each of the collectors. The designation "A" is used for results in case of the solar collector with the absorber plate made of sheet metal and the designation "B" is used for the collector with the absorber plate consisting of the CSM panels filled with the PCM. The air temperature was measured in three points along the length of the air cavities (in the direction of airflow). The temperature of the light-weight solar absorber plate was essentially the same on both sides of the plate; therefore, the temperature sensors were installed only on the non-insolated side of the solar absorber plate.

## 3.1 CLIMATIC CHAMBER EXPERIMENTS

Some outdoor experiments have been performed and their results are presented in the unabridged version of the thesis. Nevertheless, in order to investigate the behavior of the solar collectors under a specific set of climatic conditions (ambient temperature, solar radiation intensity, etc.) the outdoor experiments would have to be run for an extended period of time. On the other hand, the controlled environment of a climatic chamber is particularly suitable for experiments under a specific set of boundary conditions. The experimental air solar collectors were not designed for real-life operation, only as an experimental platform for the investigation of latent heat thermal energy storage in the solar absorber plate. The experimental collectors were not rain proof and as such could not be used in long-term investigations in outdoor environment.

The climatic chamber experiments were performed in a drive-in environmental chamber of the NETME center at the Faculty of Mechanical Engineering. The indoor air temperature in the environmental chamber can be controlled in the range from -40 °C to 85 °C. The chamber is equipped with a solar simulator consisting of six lamps on a movable frame. The output of the lamps can be controlled from about 30% of their nominal output to 100% of their nominal output. The solar simulator was designed to provide the uniform radiation intensity of 1000 $W \cdot m^{-2}$ of the spectrum similar to solar radiation in the area of 2 m by 1.5 m at the distance of 1 m from the lamps. The radiation intensity decreases with the increasing distance from the lamps. As the uniformity of the radiation intensity deteriorates with the increasing distance from the lamps, it was necessary to measure the distribution of the radiation intensity over the collector surfaces.

Fig. 9 shows the experimental air solar collectors inside of the environmental chamber. The collectors were positioned in a way that the solar absorber plates were parallel with the plane in which the lamps were installed. Since it was not possible to position the collectors in the distance of 1 m from the lamps of the solar simulator, the collectors were positioned at the distance of 2 m where the radiation intensity was just over 600 $W \cdot m^{-2}$. The radiation intensity, while lower than that used in the standard collector testing, was sufficient for the purpose of the experiments. The collectors placed side by side had the overall dimensions of 2 m by 1.5 m and could be positioned in the central part of the irradiance field with relatively good uniformity of radiation intensity.

***Fig. 9*** *Experimental collectors in the climatic chamber*

The experiments were performed for solar heating of ventilation air. It means that the ambient air was drawn into the collector and thus the ambient air temperature was the inlet air temperature. Fig. 10 shows the results of one of the experiments carried out at a subzero ambient temperature. The indoor space of the climatic chamber was cooled down to -5 °C and then the solar simulator was switched on to the maximum output (100%). As can be seen, the solar simulator influenced not only the air temperatures at the outlet of the air solar collectors (Aout and Bout) but also the inlet air temperature (Ain and Bin). The constant radiation intensity was maintained for about 10 hours while three air flow rates were tested (125 $m^3 \cdot h^{-1}$, 95 $m^3 \cdot h^{-1}$, 65 $m^3 \cdot h^{-1}$). The changes of the airflow rates translated into changes of the outlet air temperature. The air temperature at the outlet of the collectors exceeded 20 °C for the smallest air flow rate. Both the solar simulator and the cooling system of the environmental chamber were switched off just after 7 P.M. The air temperature in the chamber began to increase and since the fans in the air collectors kept running all temperature sensors soon indicated almost the same temperature.

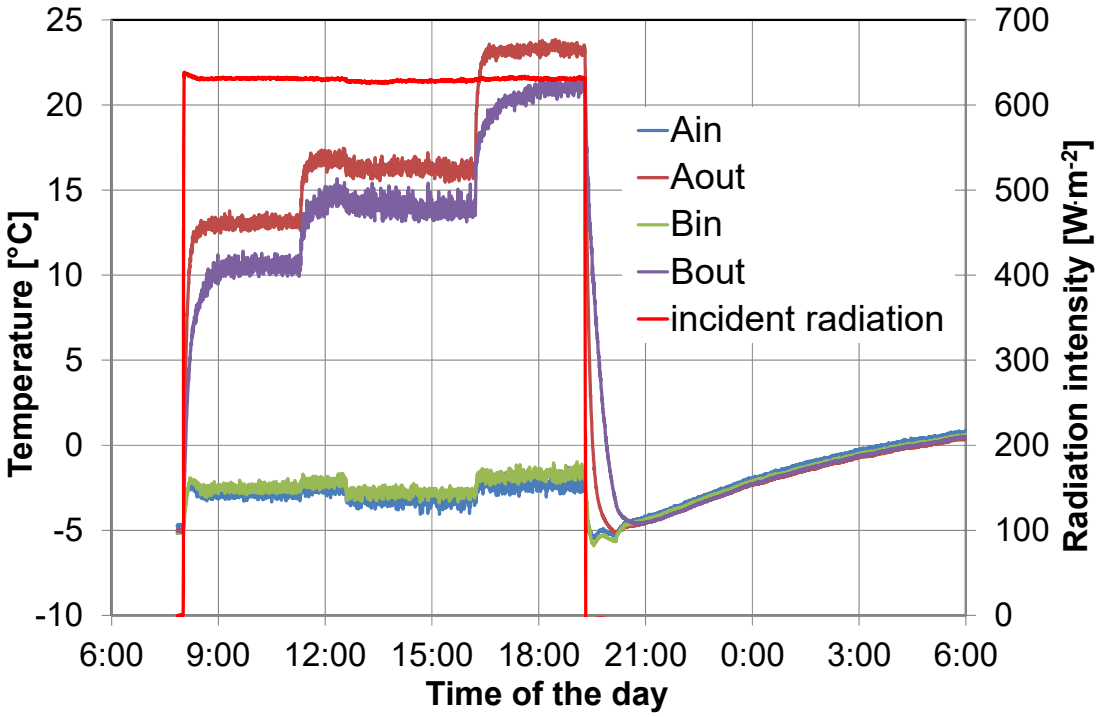


***Fig. 10*** *Inlet and outlet air temperatures*

The useful heat gains of the collectors at the steady-state operating conditions are shown in Fig. 11. The useful heat gain was calculated from the mass flow rate of air passing through the collectors and the difference between the inlet and outlet air temperature.

$$\dot{Q}_u = \dot{m}_a \, c_{pa} \, (T_{coll.out} - T_{coll.in}) \qquad (2)$$

where $\dot{m}_a$ is the mass flow rate of air, $c_{pa}$ is the average value of specific heat of air, $T_{coll.out}$ is the air temperature at the outlet of the collector and $T_{coll.in}$ is the air temperature at the inlet of the collector. Three time intervals were used for the evaluation of the steady-state performance of the collectors: 9:00 to 11:00 for the air flow rate of 125 $m^3 \cdot h^{-1}$; 12:00 to 16:00 for the air flow rate of 95 $m^3 \cdot h^{-1}$; and 18:00 to 19:10 for the air flow rate of 65 $m^3 \cdot h^{-1}$. As can be seen in Fig. 11 the useful heat gain of the solar collector with the light-weight absorber plate was higher than the useful heat gain of the collector with the solar absorber plate containing PCM.

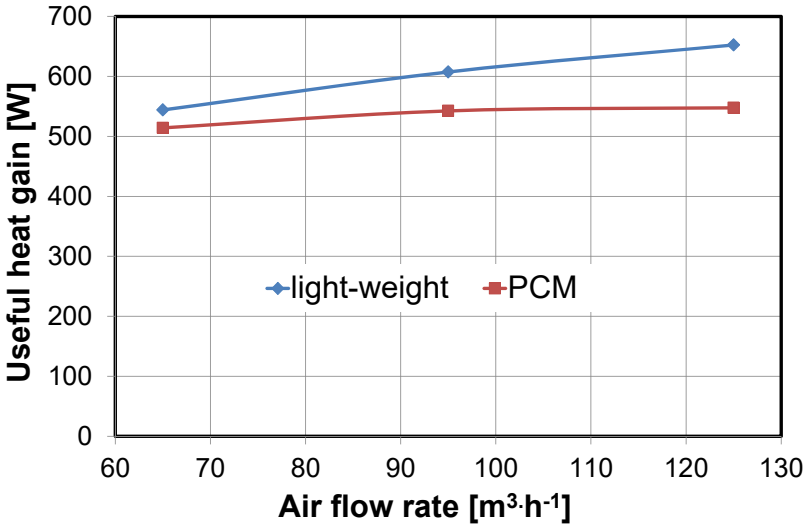


***Fig. 11*** *Useful heat gains of the collectors*

The situation is quite similar in case of the efficiency of the collectors under the tested operating conditions, see Fig. 12. The thermal efficiency of a solar collector is defined as

$$\eta = \frac{\dot{Q}_u}{A\,G} \tag{3}$$

where $\dot{Q}_u$ is the useful heat gain, $A$ is the area of the collector and $G$ is the total solar radiation incident on the collector area.

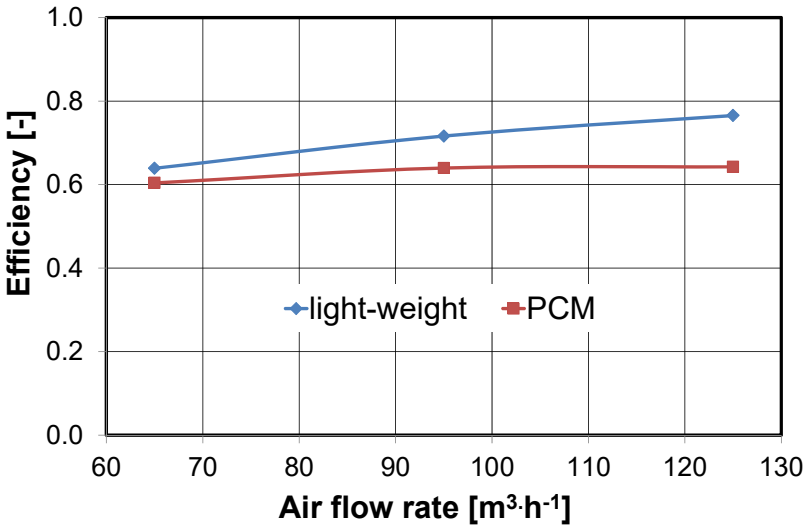


***Fig. 12*** *Thermal efficiency of the collectors*

The efficiency of the collectors was relatively high considering their very simple design. One of the reasons was the operation of the collectors in the fresh air (ventilation air) heating mode in which the ambient air is drawn into the collectors and thus the inlet air temperature is the same as the ambient temperature. If the collectors operated in the space heating mode with the inlet air temperature of (for example) 20 °C and the ambient temperature of -5 °C the heat loss of the collectors would be much higher resulting in a lower efficiency. As can be seen in Fig. 12 the efficiency increases with the increasing air flow rate as the higher air flow rate means lower air temperature in the collectors and thus a lower heat loss.

The steady-state operating conditions are quite rare in real-life operation of air solar collectors. Both the ambient temperature and the solar radiation intensity change all the time in the outdoor environment. The solar radiation intensity in particular can change quite significantly in a short period of time. A simplified experiment was carried out in the climatic chamber to investigate the behavior of the experimental air solar collectors under changing radiation intensity. The square wave changes of the radiation intensity were used in the experiment. The square wave changes were chosen because they could be easily introduced with the solar simulator. Another reason was the possibility to investigate the response of the collectors to the sudden changes of the radiation intensity. The radiation intensity was changed with a period of 30 minutes. The solar simulator can operate with a feedback adjusting the radiation intensity to the desired level with the use of a feedback pyrometer. However, as it takes some time for the solar simulator to reach the desired radiation intensity, it was decided to simply switch between the maximum and minimum output of the solar lamps. That was approximately between 30% and 100% percent of the nominal output of the solar simulator, as such were the limits of the solar lamps. It would also be possible to switch the simulator (the solar lamps) on and off repeatable. However, since solar radiation intensity never decreases to zero when a cloud passes over the sun such experiments would be really far from the reality. The results of the experiment can be seen in Fig. 13. The radiation intensity was kept constant for more than four hours in order to bring the collectors to the steady-state conditions. Then the square wave changes of radiation intensity were introduced.

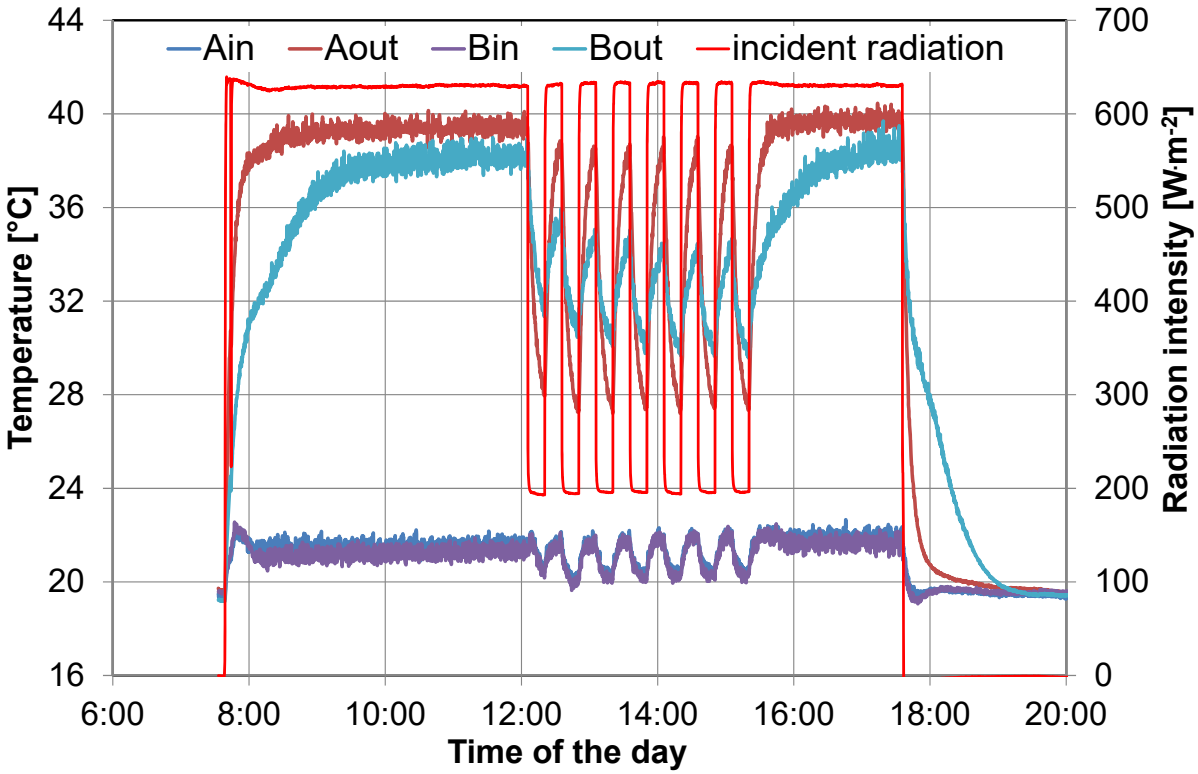


***Fig. 13*** *Square wave changes of radiation intensity*

The ambient air temperature (air temperature in the environmental chamber) was maintained at 20 °C in this experiment. The reason for such a high ambient temperature, which was also the inlet air temperature of the collectors, was to make sure that most of the PCM would be in the liquid state before the square wave changes of the radiation intensity were introduced. The air temperature in the vicinity of the inlets of the collectors was again influenced by operation of the solar simulator, as can be seen in Fig 13.

### 3.2 NUMERICAL SIMULATIONS

There are generally two approaches to the numerical simulation of the behavior of solar collectors. In the first approach a numerical model that addresses all forms of heat and mass transfer that take place in the solar collector is created. Such a model requires the detailed knowledge of the design of the solar collector. The second approach utilizes experimentally obtained performance characteristics of a solar collector. The detailed knowledge of the design of the collector is not needed in this approach as the simulation model uses the mathematical description of the performance of the collector based on the experimental data. Both approaches to simulation of the performance of solar collectors can be used in the optimization studies where a set of input parameters is changed according to an optimization algorithm with the aim to find and optimal solution [13], [14].

The model of the experimental air solar collectors was developed in parallel with the experiments; therefore, the first of the above described approaches had to be used. The TRNSYS vs. 17 was employed as a simulation tool. A combination of the existing models available in TRNSYS with an in-house model of the latent heat storage in the solar absorber plate was used. The schematic of the simulation model is shown in Fig. 14.

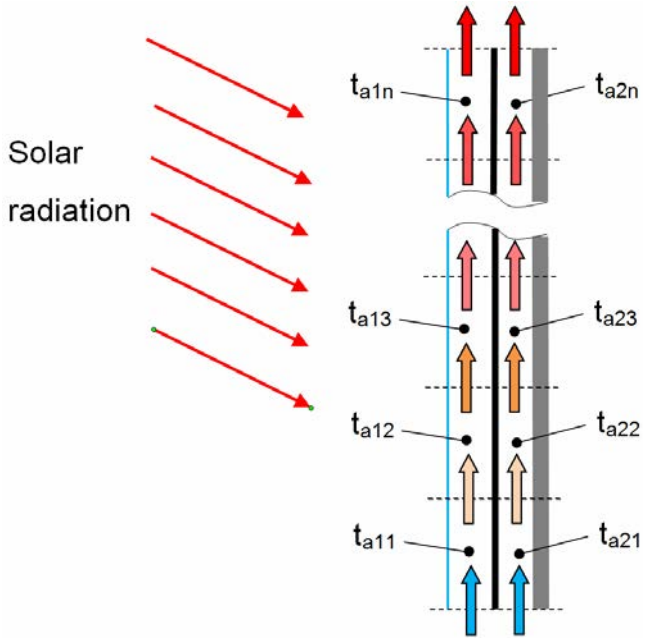


***Fig. 14*** *Schematic of the simulation model of the air solar collector*

The model was implemented as one-dimensional (1D). Each air cavity was divided into *n* sections with respective calculation air nodes ($t_{a11}$ to $t_{a1n}$ for the insolated air cavity and $t_{a21}$ to $t_{a2n}$ for the non-insolated air cavity). Heat transfer through the solar absorber plate was solved for each section separately. The already mentioned TRNSYS type was developed for the solution of heat transfer through the solar absorber plate with PCM. A simplified schematic of the computational domain is shown in Fig. 15. The thickness of the PCM layer in the solar absorber plate was 10 mm in the studied case but the model was formulated in a way that the user could specify both the thickness of the layer and the number of nodes in the layer. The following boundary conditions were used on the insolated side of the absorber plate; the solar radiation intensity incident on the surface of the absorber, the air temperature, and the heat transfer coefficient. The combination of the air temperature and the heat transfer coefficient constituted the boundary conditions on the non-insolated side of the solar absorber plate. All boundary conditions were specified as variables, it means that they could change in every time step.

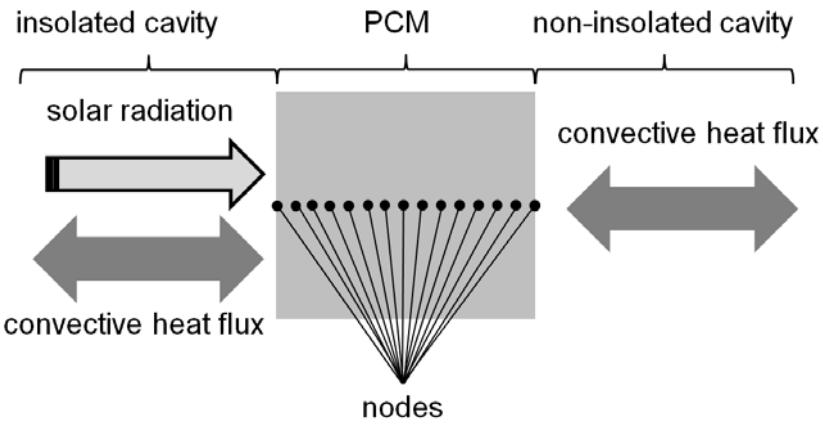


***Fig. 15*** *Schematic of the computational domain*

The computational domain shown in Fig. 15 was solved for each section shown in Fig. 14. In this manner a three-dimensional problem can be solved as a series of one-dimensional problems.

Many papers dealing with numerical modeling of phase change materials have been published in the last decade. Dutil et al. [15] and Liu et al. [16] provide quite a substantial review of various approaches to simulation of PCMs. The numerical model, used for heat transfer in the solar absorber plate with PCM, was based on the implementation of the 1D heat transfer equation that includes an internal source of heat [17]

$$\rho c \frac{\partial T}{\partial \tau} = \frac{\partial}{\partial x}\left(k \frac{\partial T}{\partial x}\right) + \dot{Q} \tag{4}$$

where $\rho$ is the density, $c$ is the specific heat, $k$ stands for the thermal conductivity, $\tau$ is time, $T$ represents the temperature, and $x$ is the spatial coordinate (in the direction of the thickness of the PCM layer). The internal heat source of the latent heat of fusion $Q$ in Eq. (4) can be expressed as follows [18],

$$\dot{Q} = \rho \, H_m \frac{\partial f_s}{\partial \tau} \tag{5}$$

where $H_m$ denotes the latent heat of fusion and $f_s$ is the solid fraction. The solid fraction represents the ratio between the solid and liquid phases ($0 \leq f_s \leq 1$). When all PCM is in the liquid state then $f_s = 0$, when all PCM is in the solid state $f_s = 1$. The effective heat capacity method [19] was adopted as an approach to modelling of the phase change (absorption and release of latent heat). This method makes use of the effective heat capacity $c_{eff}$ in order to comprise the latent heat of fusion. The effective heat capacity can be defined as follows,

$$c_{eff}(T) = \frac{1}{\rho}\frac{\partial H}{\partial T} = c - H_m \frac{\partial f_s}{\partial \tau}\frac{\partial \tau}{\partial T} \tag{6}$$

where $H$ is the enthalpy. Hence, the effective heat capacity is proportional to the slope of the enthalpy function with respect to the temperature. The substitution of Eq. (6) into Eq. (4) results in the governing equation of heat transfer in the PCM as follows

$$\rho c_{eff} \frac{\partial T}{\partial \tau} = \frac{\partial}{\partial x}\left(k \frac{\partial T}{\partial x}\right) \tag{7}$$

A general dependence of the effective heat capacity on the temperature of the material undergoing a phase change can be seen in Fig. 16. The effective heat capacity is the same as the specific heats in the liquid and solid states of the material outside of the phase change temperature range. The effective heat capacity significantly varies when the material undergoes phase change as it comprises the absorption or the release of latent heat.

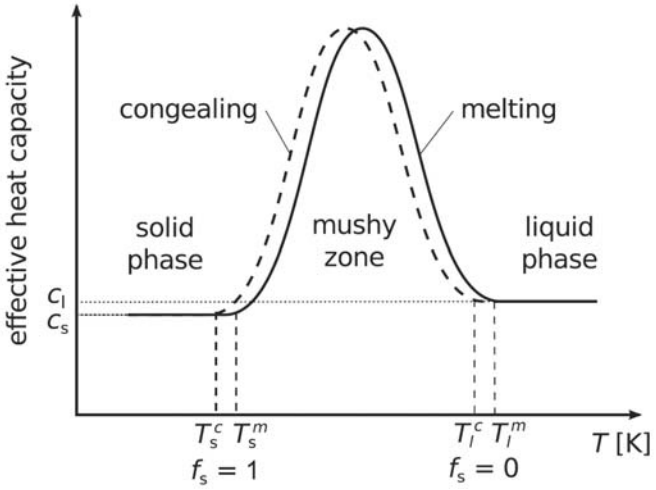


***Fig. 16*** *Effective heat capacity [20]*

The temperature range of the phase change, in which both the solid and liquid phases simultaneously coexist and the solid fraction satisfies $0 < f_s < 1$, is commonly called the mushy zone [18]. Fig. 16 shows the effective capacity for a material with a phase change hysteresis that is rather typical for most of the PCMs. The hysteresis complicates numerical modelling of the thermal behavior of PCMs when the material does not fully liquefy or solidify during a heat storage cycle. The effective heat capacity of a PCM is usually determined experimentally, e.g. with the use of the differential scanning calorimetry method [21] or utilizing the thermal delay method [22]. A simplified approach as described by Kuznik et al. [23] was utilized in the numerical simulations presented in this thesis. The effective heat capacity of Rubitherm RT42 was proposed in the form of a Gaussian-shaped function. The specific heat in solid and liquid state was considered to be the same $c_s = c_l = c_0$. The effective heat capacity function reads as follows,

$$c_{eff}(t) = c_0 + c_m \, exp\left\{-\frac{\left(T - T_{pch}\right)^2}{2.1}\right\} \tag{8}$$

where $c_0$ is specific heat and $c_m$ is the maximum increment of the specific heat due to the latent heat. The mean temperature of the phase change $T_{pch}$ for melting and congealing was considered to be $t_m = 41$ °C and the specific heat $c_0 = 2$ kJ·kg$^{-1}$·K$^{-1}$. The effective heat capacity defined in Eq. (8) gives a good agreement with the material properties stated in the RT42 data sheet (Table 1). The product data sheet did not directly specify the latent heat of the solid–liquid phase change. Instead, the heat storage capacity in a temperature range around the melting point (between 35 °C and 50 °C) was specified with the uncertainty of 7.5%. It means that the heat storage capacity of RT42 between 35 °C and 50 °C was 174 ± 13 kJ kg$^{-1}$K$^{-1}$.

As for the specific heat, it primarily depends on the chemical composition of a PCM. The specific heat in both the solid and the liquid state is between 1 kJ·kg$^{-1}$·K$^{-1}$ and 2.5 kJ·kg$^{-1}$·K$^{-1}$ for the majority of commercially available PCMs, [24]. The specific heat in the solid and liquid state of Rubitherm RT42 (in the product datasheet) was 2 kJ·kg$^{-1}$·K$^{-1}$.

***Table 1*** *Properties of RT 42*

| | |
|---|---|
| Melting temperature range | 38 °C – 43 °C<br>typical 41 °C |
| Congealing temperature range | 43 °C – 37 °C<br>typical 42 °C |
| Heat storage capacity (between 35 °C and 50 °C) | 174 $kJ \cdot kg^{-1}$ |
| Density in solid state at 15 °C | 880 $kg \cdot m^{-3}$ |
| Density in liquid state at 80 °C | 760 $kg \cdot m^{-3}$ |
| Volume expansion (solid/liquid phase change) | 16 % |
| Heat conductivity | 0.2 $W \cdot m^{-1} \cdot K^{-1}$ |

However, Kenisarin & Mahkamov [25] reported the solid and liquid specific heats of Rubitherm RT42 of 1.8 $kJ \cdot kg^{-1} \cdot K^{-1}$ and 2.4 $kJ \cdot kg^{-1} \cdot K^{-1}$, respectively. Losada-Peréz et al. [26] determined the specific heats of Rubitherm RT42 experimentally with the use of the adiabatic scanning calorimetry method. They reported the specific heat of 3.5 $kJ \cdot kg^{-1} \cdot K^{-1}$and 2.3 $kJ \cdot kg^{-1} \cdot K^{-1}$ in the solid and liquid state, respectively. Considering the specific heat of 2 $kJ \cdot kg^{-1} \cdot K^{-1}$, the latent heat is 144 $kJ \cdot kg^{-1} \cdot K^{-1}$, which is also consistent with the findings of Kenisarin & Mahkamov. Considering the uncertainty of ±7.5% for the heat storage capacity, two $c_{eff}(t)$ curves for the borders of the uncertainty interval can be used. The parameters of the curves are presented in Table 2.

***Table 2*** *Parameters of effective heat capacity curves*

| | $c_m$ [$kJ \cdot kg^{-1}K^{-1}$] | Heat storage capacity (35°C to 50°C) [$kJ \cdot kg^{-1}K^{-1}$] | Latent heat of phase change [$kJ \cdot kg^{-1}K^{-1}$] |
|---|---|---|---|
| Lower uncertainty level (−7.5%) | 51.1 | 161 | 131 |
| Mean | 56.2 | 174 | 144 |
| Upper uncertainty level (+7.5%) | 61.3 | 187 | 157 |

In comparison to the enthalpy method [27], [28], [29], which can also be used for modelling of phase change problems, the effective heat capacity approach requires only the primary unknown variable – the temperature – that is calculated directly from Eq. (7). Another advantage of the effective heat capacity approach is the possibility to use an implicit discretization scheme, and therefore, unlimited time step of simulation due to the unconditional numerical stability [30]. However, to ensure a desired accuracy the time step is still limited by the narrow temperature interval of the mushy zone where the effective heat capacity changes rapidly.

The control volume method using the explicit scheme for the time derivative was utilized in order to solve the problem numerically [31]. Due to the conditional stability of the explicit time discretization, the time step of the simulation was carefully determined with the use of the stability criteria in order to prevent numerical instability or oscillations [32].

### 3.3 RESUTS

Fig. 17 shows the simulated outlet air temperature of the collector with the light-weight solar absorber plate for the experiment with the square-wave changes of solar radiation intensity, see Fig. 13. The measured values of the inlet air temperature and the radiation intensity were used as inputs in the simulation.

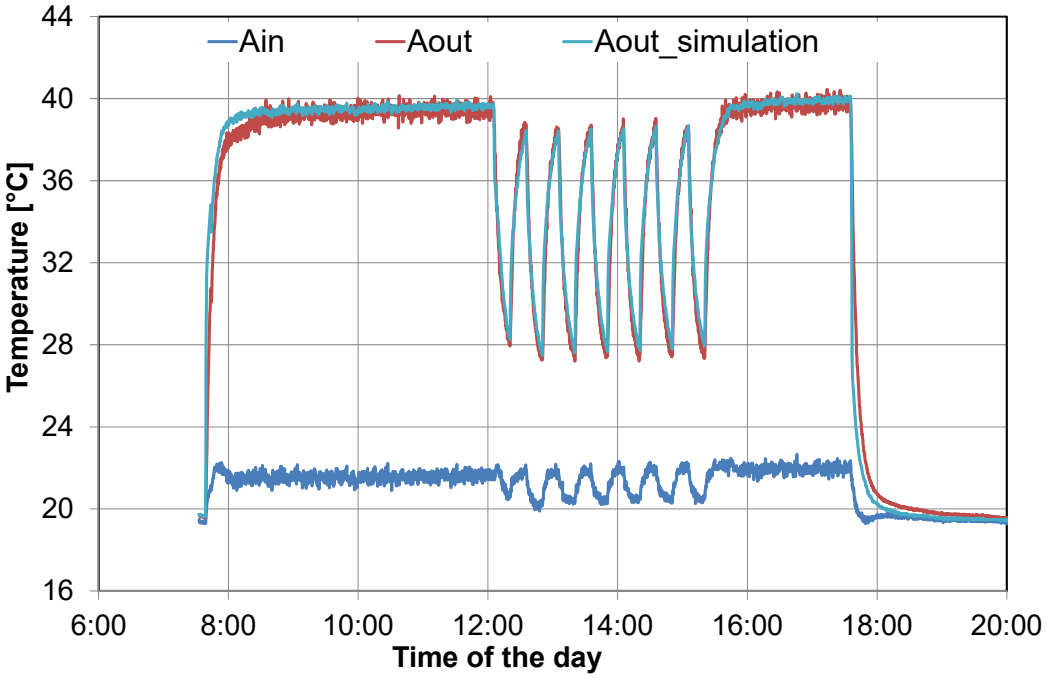


***Fig. 17*** *Simulated outlet air temperature – light-weight absorber plate*

The simulation results for the air solar collector with the solar absorber plate containing the PCM are in Fig. 18.

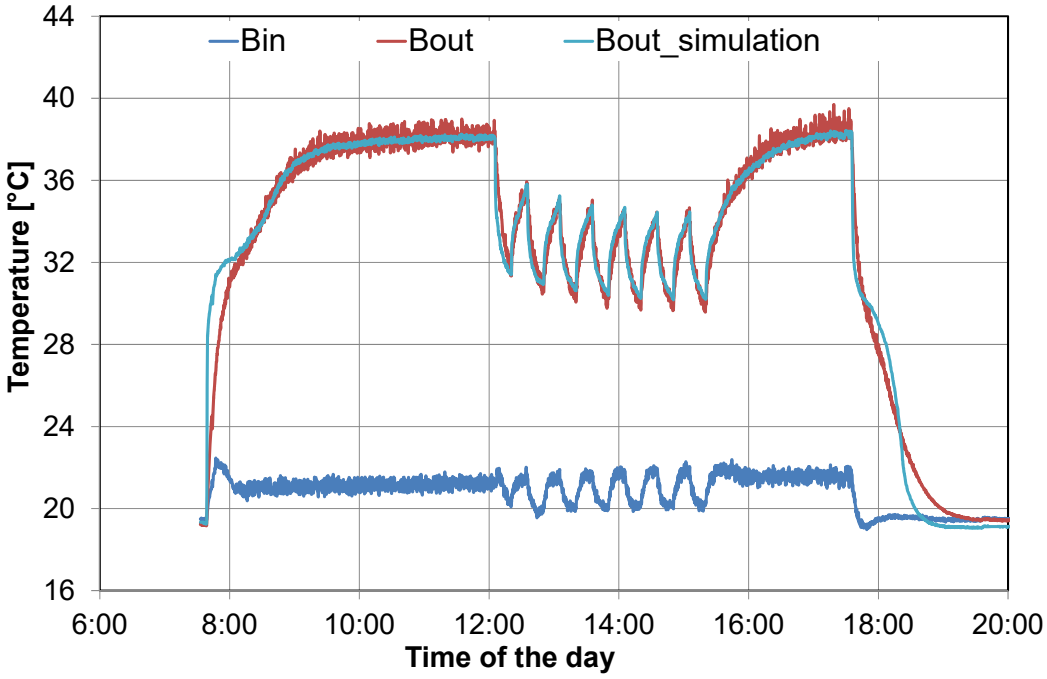


***Fig. 18*** *Simulated outlet air temperature – absorber plate with PCM*

The agreement between the numerical and experimental results is rather good under the steady-state conditions but some discrepancies can be observed for the dynamic changes of boundary conditions. Nonetheless, considering the simplification to a 1D case the agreement between the experimental and numerical results is quite good. Both experimental and numerical results have shown that integration of latent heat thermal energy storage with the solar absorber plate of an air solar collector reduces the changes of outlet air temperature under varying solar radiation intensity. However, the thermal resistance of the solar absorber plate with the PCM resulted in worse efficiency in comparison to the collector with the light-weight solar absorber plate.

# 4 HEAT STORAGE IN SOLAR AIR HEATING

This chapter contains the work already published in [20]. Thermal energy storage in solar air heating systems is mostly intended to provide the heat storage capacity for hours or days of operations. Since the volumetric thermal capacity of water is approximately 3500-times higher than that of air it makes much more sense to use water-based solar heating systems when long-term (e.g. seasonal) thermal energy storage is needed and to employ water-to-air heat exchangers for air heating. The aim of the study presented in this chapter was to develop and validate a simulation model for a heat storage unit comprising CSM panels filled with PCMs.

Several studies, both experimental and numerical, were carried out into latent heat thermal storage with air as a heat transfer fluid. Hed & Bellander [33] reported mathematical modelling of a PCM-air heat exchanger for thermal storage in case of night cooling. The model was implemented as a single node finite difference model. The heat loss to the ambient environment was neglected. The authors used the model to investigate the influence of the surface roughness on heat transfer rates in the heat storage unit. The authors concluded that the rough surface can significantly intensify heat transfer between the fluid and the heat storage material, but this intensification is subsequently paid for by a higher fan power. Modelling and experimental validation of a similar arrangement of a PCM-air heat exchanger for free cooling applications was presented by Lopez et al. [34]. The authors considered an exchanger consisting of parallel horizontal PCM slabs with air gaps between the slabs. The simulation model was created in MATLAB with the use of control volume method. The same air flow rates were considered in all air gaps and thus only a half of the slab thickness with a half of the air gap was modelled. The heat loss to the ambient environment was neglected.

A quite extensive study of a PCM-air heat exchanger containing aluminum containers filled with a PCM (compact storage modules – CSM) was presented by Dolado et al. [6]. The authors studied a PCM-air exchanger in which the CSM panels were positioned vertically and the direction of air flow was also vertical with air supply at the top of the heat storage unit and the air return at its bottom. The paraffin-based PCM RT27 was used in the investigations. The total weight of the PCM in the unit was 135 kg. Both an empirical model [6] and a numerical model [35] of the investigated heat storage unit were developed. The numerical model of the PCM layer was developed with the use of finite difference method as a one-dimensional implicit formulation. Halawa & Saman [36] reported the thermal performance analysis of a phase change thermal storage unit for space heating. The PCM used in the study was calcium chloride hexahydrate (referred to as PCM29 in the paper) with the melting temperature of 28 °C. The PCM-air heat exchanger consisted of parallel slabs in a rectangular duct with air passing between the slabs. The authors analyzed the influence of various parameters such as the air flow rate, the PCM slab thickness or the air gap on the performance of the unit. The adiabatic walls of unit were considered (no heat loss to the ambient environment). Such an assumption is only reasonable for a parametric study in which the influence of various design and operation parameters is investigated. Moreover, the PCM melting temperature of 28 °C seems to be relatively low for space heating applications.

## 4.1 EXPERIMENTAL HEAT STORAGE UNIT

A lab-scale LHTES unit was built for experimental investigations and for the validation of the simulation model. The experimental LHTES unit was intended for a day-cycle operation in which both heat charging and heat discharge take place within a 24-hour interval. The main goal in such operation is to shift solar heat gains from daytime to after sunset. On certain days, especially in spring and autumn, space heating or ventilation air heating is not needed during daytime when the outdoor air temperature is relatively high and solar radiation is available, but the need of space heating may arise after sunset. Likewise, some residential buildings do not need to be ventilated or heated up to the comfort level during the day because the occupants are not at home. These are the situations where a day-cycle LHTES unit can be used in solar air heating. Solar heat can be stored in the LHTES unit during the day, when the heat supply exceeds the heat demand, and it can be released after sunset.

The CSM panels provide a rather easy and flexible approach to building LHTES units of a desired thermal storage capacity. The CSM panels can be arranged in various ways in the units. The basic arrangement is a row of parallel CSM panels with an air channel between the two adjacent panels. In order to increase the capacity of the heat storage unit the CSM panels can be added in all three spatial directions. The basic configuration of the experimental heat storage unit can be seen in Fig. 19.

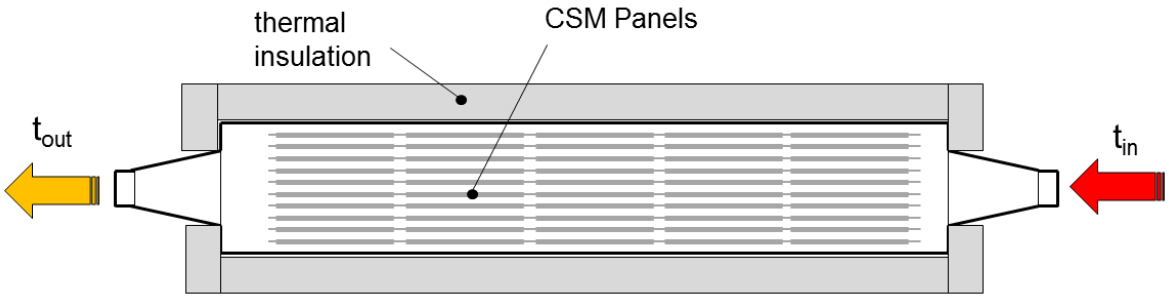


***Fig. 19*** *Experimental heat storage unit [20].*

The unit contained 100 CSM panels filled with the RT42. The properties of RT42 as specified in the product data sheet were summarized in Table 1 [11]. The internal dimensions of the unit were 0.44 m × 0.62 m × 1.8 m. The CSM panels had the dimensions of 450 mm × 300 mm × 10 mm and each of them accommodated approximately 700 ml of PCM. The panels were arranged in 5 rows with 20 panels in each row. The CSM panels were positioned 30 mm from each other. As the panels were 10 mm thick there was a 20 mm air gap (air channel) between the panels.

The PCM-air heat storage units are generally PCM-air heat exchangers and thus they can be characterized by many parameters used for the heat exchangers, among them the surface area density. The surface area density is the ration between the heat exchange area of a heat exchanger and its volume. In case of the experimental LHTES unit the surface area density was 53 $m^2 \cdot m^{-3}$. This value is comparable with the industrial shell-and-tube heat exchangers that have the surface area density between 50 $m^2 \cdot m^{-3}$ and 100 $m^2 \cdot m^{-3}$ [38]. For the specific heat of 2 $kJ \cdot kg^{-1} \cdot K^{-1}$ in both the solid and the liquid state, as specified in the product data sheet, the overall heat storage capacity of the CSM panels (including the aluminum containers) was 11.8 MJ (3.3 kWh) in the temperature interval between 25 °C and 55 °C ($\Delta T = 30$ K). If each of the panels was filled with 700 ml of water instead of Rubitherm RT42 the total thermal storage capacity of the panels would be 9.7 MJ (2.7 kWh). It is obvious that the use of PCM-based thermal energy storage in this case only makes sense if the operation temperature range is relatively narrow.

## 4.2 EXPERIMENTAL INVESTIGATIONS

The experimental investigations of the performance of LHTES unit were carried out in a lab environment. The experimental set-up can be seen in Fig. 20. An electric heater substituting a solar air heater (collector) was used to heat up the air at the inlet of the unit. The electric heater had the maximum heating output of 2 kW. The heating output of the air heater could be controlled by means of the heater controller. Nonetheless, the maximum output of the heater was used in most experiments. A fan with the flow rate control was used to maintain the constant air flow rate through the heat storage unit. The fan allowed for the maximum air flow rate of 760 $m^3 \cdot h^{-1}$. The data acquisition system involved monitoring of the airflow rate through the unit as well as the air temperature measurements at several locations. The resistance temperature probes Pt100 were used for the air temperature measurements and the anemometric probe was used for air flow rate measurements. An open-loop arrangement of the experimental set-up was used; it means that the air passing through the unit was supplied outside of the lab. A thermally insulated flexible duct was used for this purpose. The LHTES unit itself was thermally insulated with polystyrene on the outside.

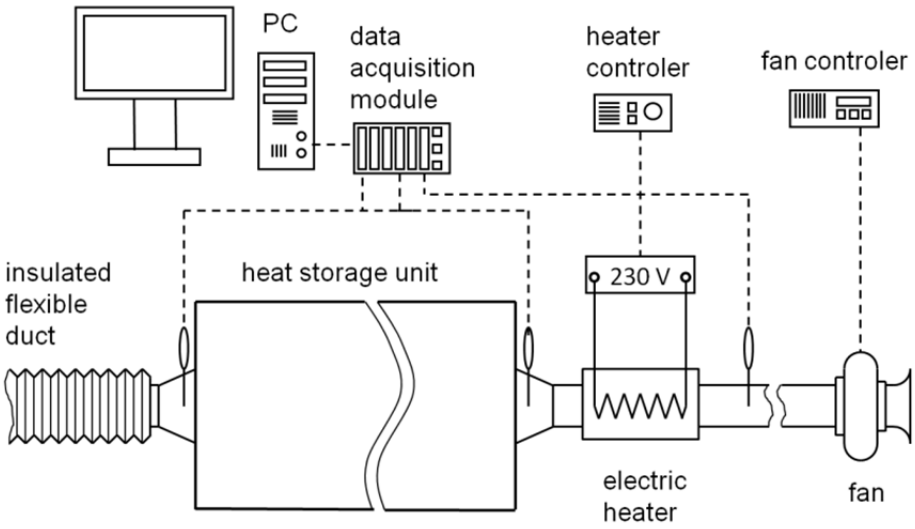


***Fig. 20*** *Experimental set-up [20].*

The application of thermal energy storage in solar air heating system means that the duration of heat charging period is limited by the availability of solar radiation. The average sunshine duration in early spring and late autumn is less than 5 hours in Brno, Czech Republic (latitude 49.2°N) and it is probably not reasonable to expect outlet temperatures of a solar air heater higher than 60 °C. It also needs to be mentioned that the temperature at the outlet of a solar air heater changes during the day and the constant outlet temperature could only be achieved for the variable airflow rate controlled with regard to the actual solar radiation and the outdoor air temperature.

One of the problems with PCM-based heat storage is the possible deterioration of the properties of PCMs over the time and with the number of undergone phase change cycles. The heat storage experiments reported in this thesis were performed for a couple of weeks with only a few dozen phase change cycles; therefore, the properties of the PCM could be assumed to be stable. The change of the PCM properties was addressed by many authors. Rathod and Banerjee [39] published the review of papers on thermal stability of PCMs used in latent heat energy storage systems. Behzadi & Farid [40] reported an irreversible physical change of the paraffin-based PCMs altering their thermophysical properties as a result of long-term exposure to the temperature above the melting point. The maximum operation temperature of RT42 specified in the product data sheet is 72 °C.

### 4.3 NUMERICAL INVESTIGATIONS

The numerical model of the LHTES unit was implemented as a quasi-one-dimensional transient heat transfer problem - similar to the air solar collector with the solar absorber plate containing PCM. The model of the unit was implemented as a type in TRNSYS 17. The development of several latent heat storage models in TRNSYS has been reported by various authors in the last decade, e.g. [41], [42], [43]. TRNSYS can be coupled with other simulation tools which increases its versatility. A coupling between TRNSYS and MATLAB was used for the development of the numerical model of the heat storage unit. Though convenient for the development of the model the coupling of MATLAB and TRNSYS is not very practical for actual simulations. For that reason, the numerical model developed in MATLAB was eventually recompiled with the use of C++ programming language to the form of the build-in TRNSYS module. The schematic of the numerical model of the heat storage unit is shown in Fig. 21.

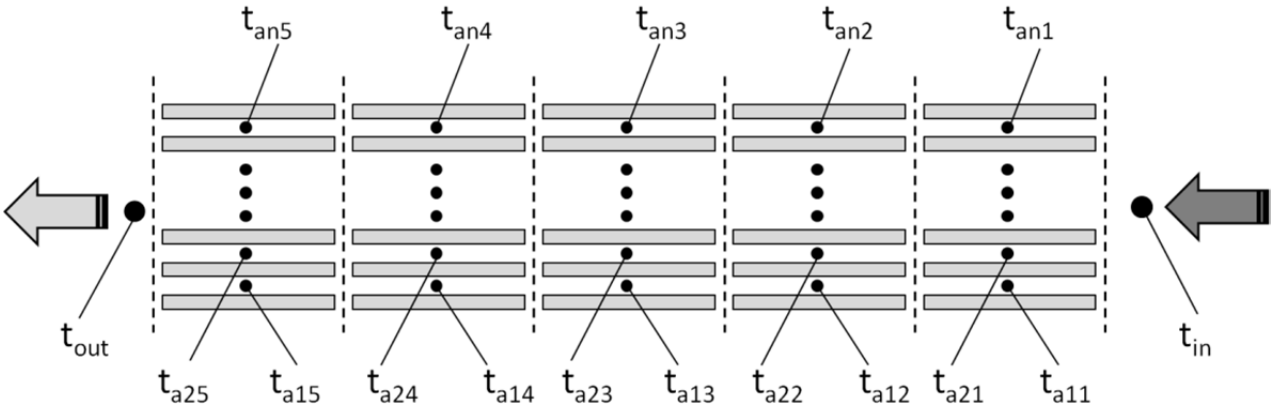


***Fig. 21****Schematic of the numerical model [20].*

The simulation of the phase change of PCM inside the CSM panels was the most time consuming part of the calculations and the computational time increased with the number of solved sections. The detail of one of the sections (computational domains) is shown in Fig. 22.

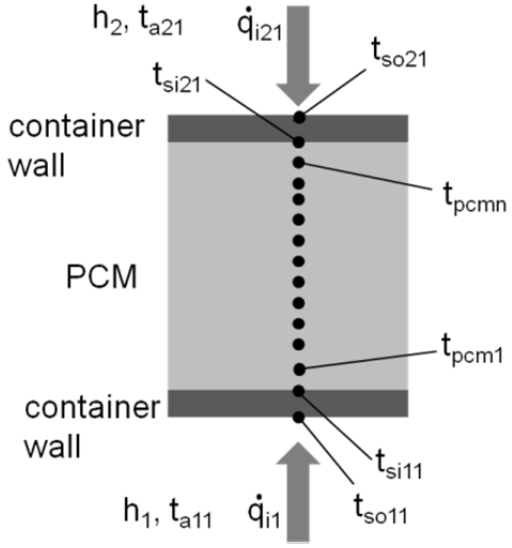


***Fig. 22*** *Schematic of a computational domain [20].*

The number of nodes used for the calculations could be specified in the model together with the number of sections which should be solved for each panel. Each section is solved as a 1D heat transfer problem. This assumption is based on the dimensions of the CSM panels where the thickness of the panel is much smaller than the other two spatial dimensions. The initial condition in the performed simulations was the uniform temperature in the entire heat storage unit. The convective heat flux, according to the Newton's law of cooling, was used as the boundary condition at the surfaces of the panels (Fig. 22). The heat transfer coefficient was determined with the use of the correlations [17] for the fluid flow between two parallel planes

$$Nu = \frac{h\,2L}{k} \tag{9}$$

where $h$ is the heat transfer coefficient, $L$ is the distance between the planes (CSM panels), and $k$ is the thermal conductivity. The Reynolds number in the investigated cases was $\mathrm{Re} \leq 1000$, which means laminar flow. The Nusselt number is constant in case of fully developed laminar flow; therefore, the heat transfer coefficient does not depend on the Reynolds number. The Nusselt number in Eq. (9) is $Nu = 8.23$ for the constant heat flux through the walls of the channel and $Nu = 7.54$ for the constant wall temperature. However, even in case of laminar flow the Nusselt number is not constant in the entry region where the flow is not yet fully developed.

## 4.4 RESULTS AND DISCUSSION

Fig. 23 shows the measured and simulated air temperatures at the inlet and outlet of the LHTES unit during the heat storage and heat release periods in the experiment with almost constant inlet air temperature.

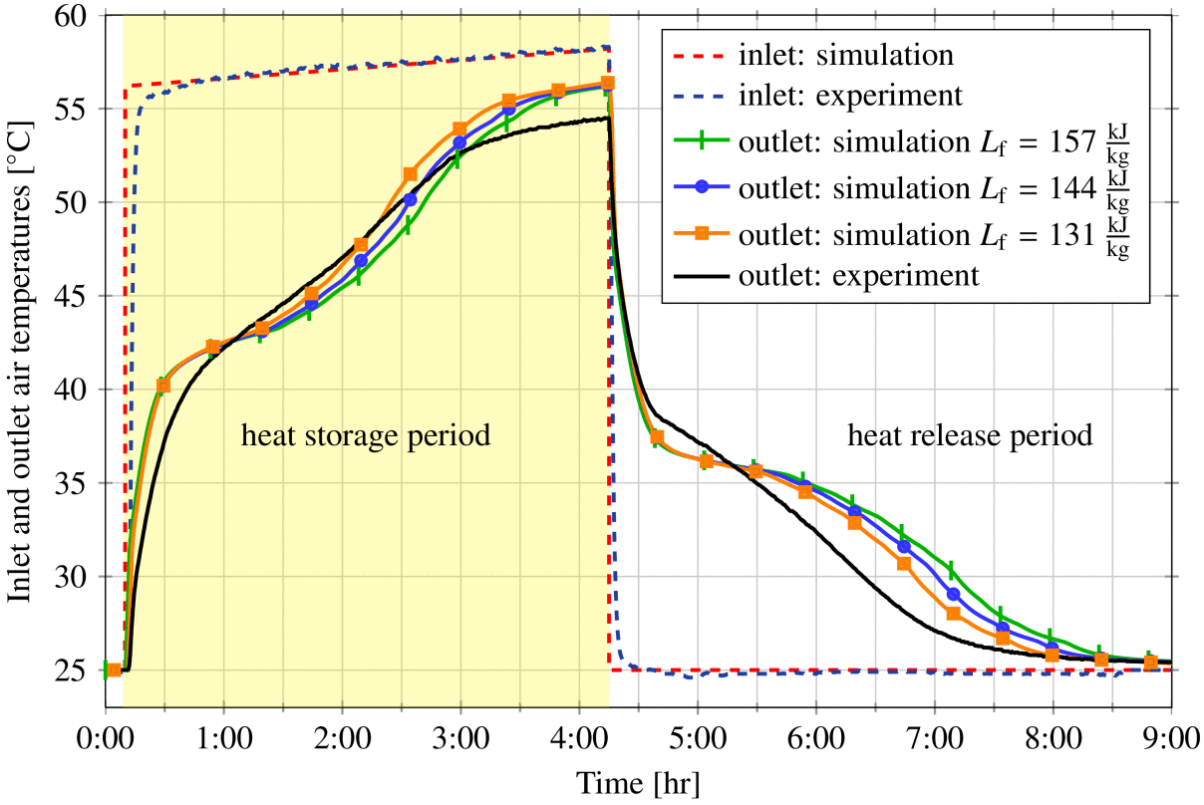


***Fig. 23*** *Inlet and outlet air temperature [20].*

The uncertainty of the value of latent heat in case of RT42, as presented in Table 2, was considered in the simulation. The heat storage period (heat charging) lasted from 0:10 to 4:15 and the heat release period (heat discharge) took place between 4:15 and 9:00. The air flow rate through the heat storage unit was 230 $m^3h^{-1}$ during the entire experiment. The experiment began from the constant temperature of the LHTES unit of 25 °C as can be seen from the inlet and outlet air temperatures in the first 10 minutes. In order to achieve this initial condition, the ambient air was circulated through the unit. Subsequently, the electric heater was switched on and almost constant inlet air temperature of 58 °C was maintained. At 4:15 the heater was switched off and the heat release period began with the inlet air temperature of 25 °C. The numerical simulations were carried out for the same initial and boundary conditions. As can be seen in Fig. 23, the outlet air temperature follows the increase of the inlet air temperature rather quickly at the beginning of the heat storage period when only sensible heat storage takes place. The onset of the melting process is clearly visible as the change in the time derivative of the outlet air temperature. Between about 0:30 and 1:00 the time derivative of the outlet air temperatures (i.e. the slope of the increase of air temperature) temporarily declined due to latent heat storage in the PCM. The similar behavior can be seen in the heat release period. The air temperature at the outlet of the LHTES unit was initially decreasing rather steeply, but when the air temperature reached the congealing temperature of the PCM, the decrease of the air temperature slowed down as the latent heat was released. The onset of melting and congealing did not occur in all CSM panels at the same time and that was one of the reasons for the absence of the temperature plateau (almost isothermal heat storage and release) so often shown in theoretical descriptions of latent heat storage. Another reason for the absence of the temperature plateau was the relatively wide melting range of RT42. The heat storage (heat charging) rate for the situation shown in Fig. 23 can be seen in Fig. 24.

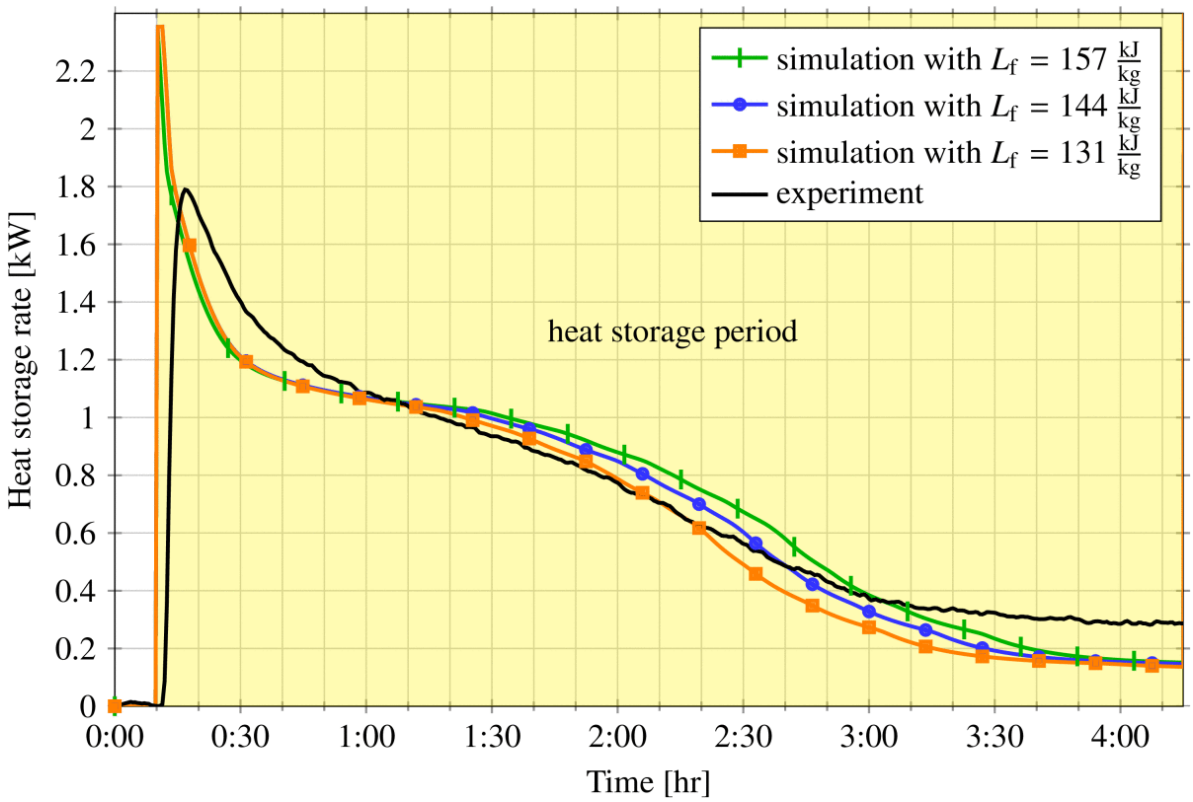


***Fig. 24*** *Heat storage rate [20].*

The heat storage rate was obtained from the air mass flow rate and the difference between the inlet and outlet air temperature

$$\dot{Q}_{in} = \dot{m}_a \, c_{pa} \, (T_{in} - T_{out}) \tag{10}$$

where $c_{pa}$ is the average value of specific heat of air at constant pressure and $T_{in}$ and $T_{out}$ are the air temperatures at the inlet and outlet of the unit as shown in Fig. 23.

The discrepancies between the simulated and measured heat storage rates at the beginning of heat storage period (from 0:10 to 0:30 in Fig. 24) are mainly due to the electric air heater. The real heater needed some time to reach the desired air temperature at the inlet of the heat storage unit. That was the reason why the peak of the heat storage rate from the experiment is not as high as in case of the numerical simulations where the inlet air temperature was reached in the first time step. The numerical model of the unit underestimated the heat loss to the surroundings. That is one of the reasons for increasing discrepancies between the experimental and numerical results over longer periods of time. At a certain point during the heat storage period the difference between the inlet air temperature and the outlet air temperature was not because of the heat being stored in the unit but only due to the heat loss to the ambient environment.

The heat release rates can be seen in Fig. 25. Similarly to the heat storage period the heat release rate was calculated as

$$\dot{Q}_{out} = \dot{m}_a \, c_{pa} \, (T_{out} - T_{in}) \tag{11}$$

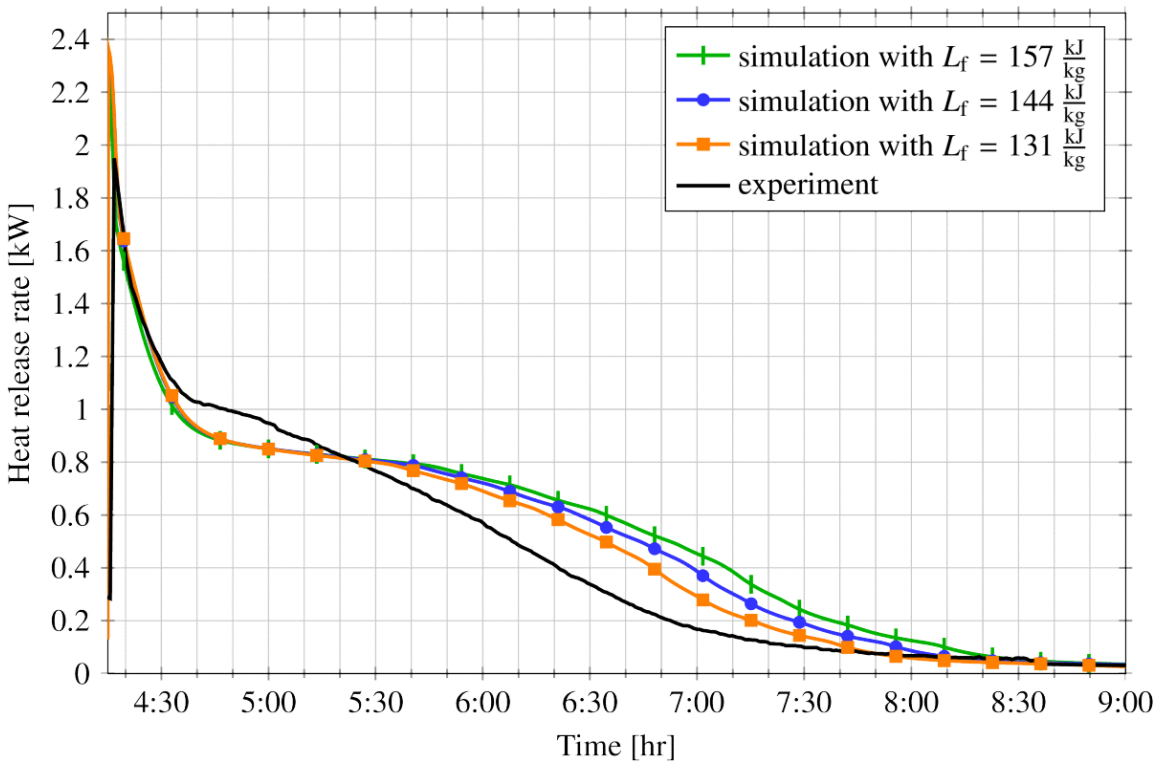


***Fig. 25** Heat release rate [20].*

The air temperature at the inlet of the unit was 25 °C during the heat release period. The air flow rate was the same as in case of the heat storage period. Again, there is a relatively good agreement between the numerical and experimental results at the beginning of the heat release period (sensible heat storage) but the discrepancies occurred when PCM began to solidify. The heat release rate peaked at around 2 kW at the beginning of the heat release period but it very quickly decreased to less than 1 kW when the sensible heat above the melting range was released. The decrease of the heat release rate was more gradual when the latent heat was released.

There are several possible reasons for discrepancies between numerical and experimental results. One-dimensional simulations require rather significant simplification of the studied problem. It means that certain phenomena cannot be addressed in detail. In case of the investigated heat storage unit the simplification mostly concerned the air flow inside the unit and the phase change of the PCM. Since the air flow in the unit could not be modelled in detail, some assumptions had to be made about the airflow rates in particular air cavities (channels). The highest air flow rate for the studied arrangement was considered in the air cavity at the horizontal midplane (plain of symmetry) of the unit and it was assumed that the air flow rate in other air cavities decreased with their distance from the midplane (with the minimum air flow rates in the air channels adjacent to the walls of the unit).

As for the phase change modelling, the 1D approach to heat transfer in the studied case seemed to be justified by the dimensions of the CSM panels where the thickness of the PCM layer was much smaller than other two spatial dimensions and the dominant heat flux could be expected in the direction of the thickness of the PCM layer. No convection was considered in the melted PCM. A 3D model of heat transfer in PCM, e.g. as used in [44] or [45], would provide much better insight into the melting process but for the computational constraints it would be very difficult to model each of the 100 CSM panels individually in 3D. The approach in which the results of a simplified 1D model are validated with experimental data and the fine-tuning of the model is done based on that comparison is probably the most feasible approach for practical application of numerical simulations at the moment.

The advantage of numerical simulations is that it is relatively easy to perform parametric studies analyzing the influence of various design and operation parameters. Fig. 26 shows the simulated outlet air temperature in the heat storage period for three levels of thermal resistance of the unit walls.

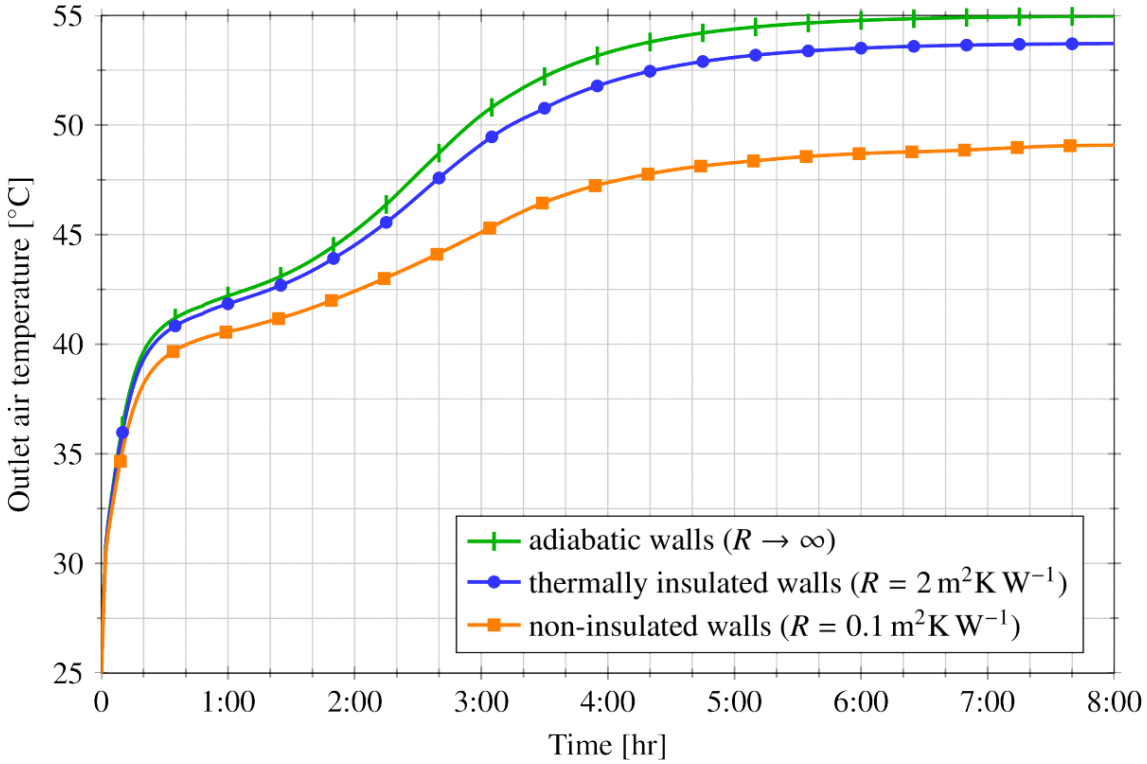


***Fig. 26*** *Heat loss of the LHTES unit [20].*

The inlet air temperature was 55 °C, the ambient temperature was 25 °C and the air flow rate was 300 $m^3 \cdot h^{-1}$. As can be seen the non-insulated unit has a rather high thermal loss. The thermal

insulation with the thermal resistance of 2 $m^2 \cdot K \cdot W^{-1}$ rather significantly reduces the heat loss. The thermal resistance R = 2 $m^2 \cdot K \cdot W^{-1}$ is equivalent to 0.1 m thick layer of thermal insulation material with the thermal conductivity of 0.05 $W \cdot m^{-1} \cdot K^{-1}$. As can be observed in Fig. 26, in case of a thermally insulated unit it is justifiable to use the assumption of adiabatic walls for the parametric studies with relatively short heat storage cycles.

The CSM panels are available with the thickness of 10 mm, 15 mm and 20 mm. The simulated outlet air temperatures during the heat storage period for LHTES units containing CSM panels of the three thicknesses are shown in Fig. 27.

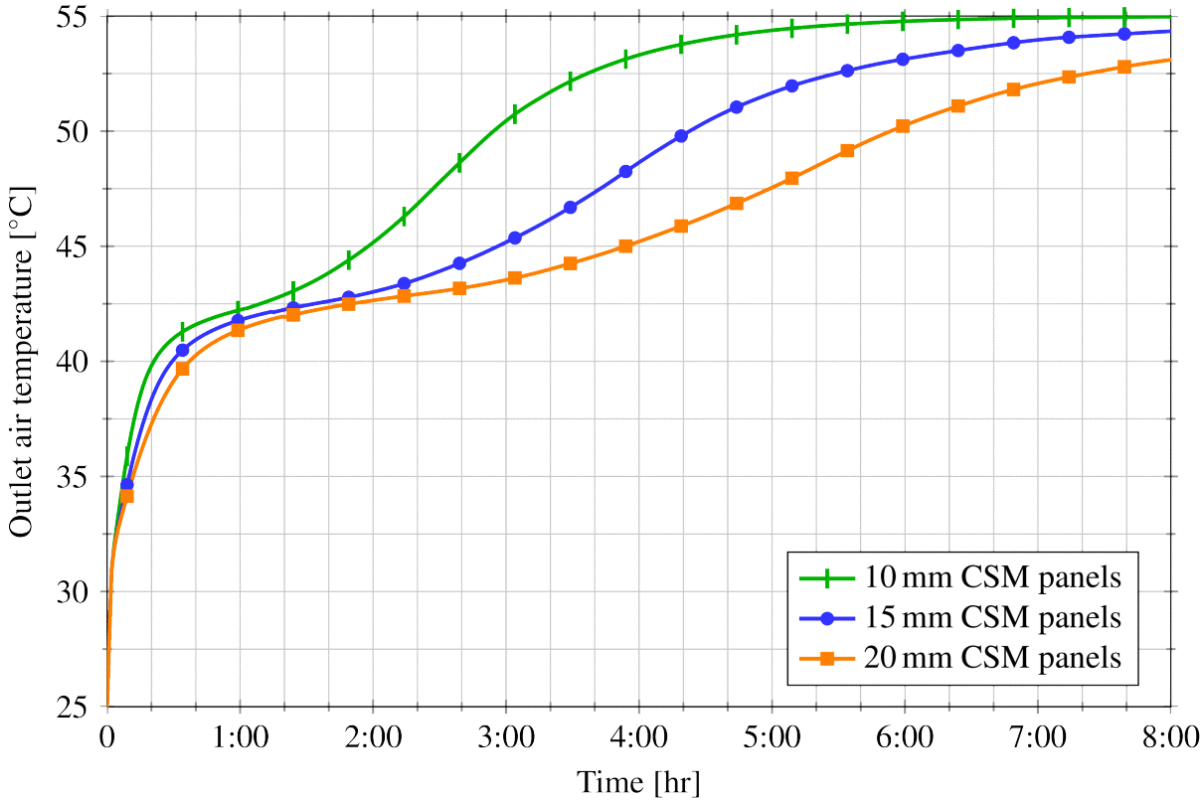


***Fig. 27*** *Different thickness of CSM panels [20].*

The simulation was carried out for the inlet air temperature of 55 °C and the air flow rate of 300 $m^3 \cdot h^{-1}$.The walls of the unit were considered adiabatic and the 20 mm wide air cavities between the panels were considered in all three cases. The use of CSM panels that accommodate larger amounts of PCM (like 15 mm and 20 mm panels) is a way to increase the thermal capacity of the LHTES unit. Another way is to use a higher number of CSM panels.

The number of parallel panels (number of panels in one row) does not influence the outlet air temperature as long as the air flow rate per panel is the same. The situation is different when the panels are added in series (e.g. 5 rows of panels as in Fig. 19). In case of a LHTES unit comprising CSM panels, the unit dimensions can only change in increments equivalent to the dimensions of the panels. For the arrangement used in the experimental unit, each row of CSM panels extends the length of the unit by 0.3 meter.

Most studies into the performance of LHTES units assume a complete phase change cycle in which the whole amount of PCM completely changes phase from solid to liquid and vice versa [33]. However, partial melting of the PCM can be commonplace in real-life operation of LHTES, especially in case of solar systems where the amount of available heat depends on solar radiation that varies significantly from day to day.

# 5 CONCLUSIONS

Energy storage is becoming a very important issue in energy management. The increasing use of variable renewable energy (VRE) sources contributes to the mismatch between production and consumption of energy. Energy storage seems to be the most viable solution to this problem at the moment. A significant part of energy consumption is in the form of heat. Heat, as the lowest form of energy, is relatively easy to store. Many heat storage techniques are already available and many more are currently under development. The investigations reported in this thesis aimed at latent heat thermal energy storage (LHTES) in solar air heating. Solar air heating brings together solar radiation, the most potent renewable energy source on Earth, and air, one of the most common heat transfer fluids on Earth.

The experiments with the air solar collectors indicated that LHTES integrated with the solar absorber plate has the potential to attenuate the fluctuations of the outlet air temperature when solar radiation intensity changes significantly. Nonetheless, the tested design of the collector with the solar absorber plate containing a phase change material (PCM) exhibited lower thermal efficiency than the collector with the light-weight solar absorber plate. The temperature of the solar absorber plate needs to be above the melting temperature of the PCM in order to make use of latent heat. Therefore, the selection of a PCM with a suitable melting temperature is important for the performance of the collectors. There are many opportunities for further investigations in this area as well as some problems to be overcome. The experiments were performed with the solar absorber plate consisting of 9 aluminum containers with a PCM. Other designs could be developed to improve heat transfer between the passing air and the PCM and also to increase heat transfer in the PCM. As the temperature of the solar absorber plate increases in the direction of air flow it could make sense to use PCMs with different melting temperature at various positions along the absorber plate.

The experiments with the LHTES unit showed that such a way of heat storage is a viable option in solar air heating. The surface area density of the LHTES unit was comparable with the industrial shell-and-tube heat exchangers but the volumetric heat storage capacity of the unit was relatively small. The narrower air channels and the use of thicker CSM panels could increase both the volumetric thermal storage capacity and the surface area density. The air temperature at the inlet of LHTES in space air heating changes much less than in case of ventilation air heating. That makes it easier to select a suitable melting temperature of the PCM for this application. The augmentation of heat transfer between the air and the heat storage modules is another topic for further research. The influence of extended heat exchange surfaces (e.g. rectangular fins) attached to the containers could be investigated. The influence of the orientation of the CSM panels in the heat storage unit is another issue for further study. The containers were positioned horizontally. Since the phase change of paraffin-based PCMs is accompanied by a significant volume change the CSM panels need to allow for that volume expansion. The liquid PCM collects in the lower part of the container and the voids can form between the PCM and the upper wall of the panels during solidification when the volume of the PCM shrinks. The voids represent thermal resistances in subsequent melting process as the PCM is not in direct contact with the wall of the container.

# REFERENCES


[1] J. Zhao, N. Liu a Y. Kang, „Optimization of ice making period for ice storage system with flake ice maker," *Energy and Buildings,* pp. 1623-1627, 2008.

[2] M. Farid, A. Khudhair, S. Razack a S. Al-Hallaj, „A review on phase change energy storage: materials and applications," *Energy Conversion and Management, 45,* p. 1597–1615, 2004.

[3] B. Zalba, J. Marin, L. Cabeza a H. Mehling, „Review on thermal energy storage with phase change: materials, heat transfer analysis and applications," *Applied Thermal Engineering, 23,* p. 251–283, 2003.

[4] J. Hadorn, „Advanced Storage Concepts for Active Solar," v *EUROSUN 2008 1st International Congress on Heating, Cooling, and Buildings*, Lisbon, 2008.

[5] A. Sharma, V. Tyagi, C. Chen a D. Buddhi, „Review on thermal energy storage with phase change materials and applications," *Renewable and Sustainable Energy Reviews,* pp. 318-345, 2009.

[6] P. Dolado, A. Lazaro, J. M. Marin a B. Zalba, „Characterization of melting and solidification in a real-scale PCM-air heat exchanger: Experimental results and empirical model," *Renewable Energy,* Sv. %1 z %236, 2906-2917, 2011b.

[7] M. Liu, W. Saman a F. Bruno, „Development of a novel refrigeration system for refrigerated trucks incorporating phase change material," *Applied Energy,* pp. 336-342, 2012.

[8] M. Pomianowski, P. Heiselberg a Y. Zhang, „Review of thermal energy storage technologies based on PCM application in buildings," *Energy and Buildings,* pp. 56-69, 2013.

[9] C. Zhao a G. Zhang, „Review on microencapsulated phase change materials (MEPCMs): Fabrication, characterization and applications," *Renewable and Sustainable Energy Reviews,* pp. 3813-3832, 2011.

[10] Y. Konuklu, M. Ostry, H. Paksoy a P. Charvat, „Review on Using Microencapsulated Phase Change Materials (PCM) in Building Applications," *Energy and Buildings,* p. doi:10.1016/j.enbuild.2015.07.019, 2015.

[11] Rubitherm, „Website of Rubitherm GmbH," 2013. [Online]. Available: http://www.rubitherm.de/. [Přístup získán 15 6 2013].

[12] G. Alvarez, J. Arce, L. Lira a M. Heras, „Thermal performance of an air solar collector with an absorber plate made of recyclable aluminum cans," *Solar Energy,* pp. 107-113, 2004.

[13] M. Yang, X. Yang, X. Li, Z. Wang a P. Wang, „Design and optimization of a solar air heater with offset strip fin absorber plate," *Applied Energy,* pp. 1349-1362, 2014.

[14] G. Notton, F. Motte, C. Cristofari a J. Canaletti, „Performances and numerical optimization of a novel thermal solar collector for residential building," *Renewable and Sustainable Energy Reviews,* pp. 60-73, 2014.

[15] Y. R. D. Dutil, N. Ben Salah, S. Lassue a L. Zalewski, „A review on phase change materials: mathematical modeling and simulations," *Renewable and Sustainable Energy Reviews 15,* pp. 112-130, 2011.

[16] S. Liu, Y. Li a Y. Zhang, „Mathematical solutions and numerical models employed for the investigations of PCMs' phase transformations," *Renewable and Sustainable Energy Reviews,* pp. 659-674, 2014.

[17] F. P. Incropera a D. P. De Witt, Fundamentals of heat and mass transfer, Wiley & Sons, 2007.

[18] D. Stefanescu, Science and Engineering of Casting Solidification, 2nd editor, New York: Springer, 2009.

[19] H. Yang a Y. He, „Solving heat transfer problems with phase change via smoothed effective heat capacity and element-free Galerkin methods," *International Communications in Heat and Mass Transfer,* sv. 37, p. 385–392, 2010.

[20] P. Charvát, L. Klimeš a M. Ostrý, „Numerical and experimental investigation of a PCM-based thermal storage unit for solar air systems," *Energy and Buildings 68,* pp. 488-497, 2014.

[21] G. Zhang a C. Zhao, „Thermal and rheological properties of microencapsulated phase change materials," *Renewable Energy,* č. 36, p. 2959–2966, 2011.

[22] E. Kravvaritis, K. Antonopoulos a C. Tzivanidis, „Experimental determination of the effective thermal capacity function and other thermal properties for various phase change materials using the thermal delay method," *Applied Energy,* pp. 4459-4469, 2011.

[23] F. Kuznik, J. Virgone a J.-J. Roux, „Energetic efficiency of room wall containing PCM wallboard: A full-scale experimental investigation," *Energy and Buildings,* pp. 148-156, 2008.

[24] F. Agyenim, N. Hewitt, P. Eames a M. Smyth, „A review of materials, heat transfer and phase change problem formulation for latent heat thermal energy storage systems (LHTESS)," *Renewable and Sustainable Energy Reviews,* pp. 615-628, 2010.

[25] M. Kenisarin a K. Mahkamov, „Solar energy storage using phase change materials," *Renewable and Sustainable Energy Reviews,* pp. 1913-1965, 2007.

[26] P. Losada-Peréz, C. Tripathi, J. Leys, G. Cordoyiannis, C. Glorieux a J. Thoen, „Measurements of heat capacity and enthalpy of phase change materials by adiabatic scanning calorimetry," *International Journal of Thermophysics,* p. 913–924, 2011.

[27] C. Swaminathan a V. Voller, „A general enthalpy method for modeling solidification process," *Metallurgical Transactions B: Process Metallurgy,* p. 651–664, 1992.

[28] M. Muhieddine, E. Canot a R. March, „Various approaches for solving problems in heat conduction with phase change," *International Journal on Finite Volumes,* p. 66–85, 2009.

[29] L. Klimeš, P. Charvát a M. Ostrý, „Challenges in the computer modelling of phase change materials," *Materiali in Tehnologije 46,* p. 335–338, 2012.

[30] F. Incropera, D. DeWitt, T. Bergman a A. Lavine, Principles of Heat and Mass Transfer, 7th editor, New York: Wiley & Sons, 2013.

[31] F. Kreith, R. Manglik a M. Bohn, Principles of Heat Transfer, 7th edition editor, Pacific Grove: CL Engineering, 2010.

[32] R. Pletcher, J. Tannehill a D. Anderson, Computational Fluid Mechanics and Heat Transfer, 3rd editor, New York: Taylor and Francis, 2011.

[33] G. Hed a R. Bellander, „Mathematical modelling of PCM air heat exchanger," *Energy and Buildings,* pp. 82-89, 2006.

[34] J. Lopez, F. Kuznik, D. Baillis a J. Virgone, „Numerical modeling and experimental validation of a PCM to air heat exchanger," *Energy and Buildings,* pp. 415-422, 2013.

[35] P. Dolado, A. Lazaro, J. Marin a B. Zalba, „Characterization of melting and solidification in a real scale PCM-air heat exchanger: Numerical model and experimental validation," *Energy Conversion and Management,* pp. 1890-1907, 2011a.

[36] E. Halawa a W. Saman, „Thermal performance analysis of a phase change thermal storage unit for space heating," *Renewable Energy,* Sv. %1 z %215, 259-264, 2011.

[37] R. Shah a D. Sekulic, Fundamentals of Heat Exchanger Design, ISBN: 978-0-471-32171-2 editor, Hoboken, New Jersey: John Wiley & Sons, 2003.

[38] M. Rathod a J. Banerjee, „Thermal stability of phase change materials used in latent heat energy systems: A review," *Renewable and Sustainable Energy Reviews 18,* pp. 246-258, 2013.

[39] S. Behzadi a M. Farid, „Long term thermal stability of organic PCMs," *Applied Energy,* pp. 11-16, 2014.

[40] M. Liu, W. Saman a F. Bruno, „Computer simulation with TRNSYS for a mobile refrigeration system incorporating a phase change thermal storage unit," *Applied Energy,* sv. 132, pp. 226-235, 2014.

[41] F. Kuznik, J. Virgone a K. Johannes, „Development and validation of a new TRNSYS type for the simulation of external building walls containing PCM," *Energy and Buildings 42,* p. 1004–1009, 2010.

[42] M. Ibanez, M. Lazaro, B. Zalba a L. Cabeza, „An approach to the simulation of PCMs in building applications using TRNSYS," *Applied Thermal Engineering 25,* pp. 1796-1807, 2005.

[43] H. Shmueli, G. Ziskind a R. Letan, „Melting in a vertical cylindrical tube: numerical investigation and comparison with experiments," *International Journal of Heat and Mass Transfer,* pp. 4082-4091, 2010.

[44] F. Tan, S. Hosseinizadeh, J. Khodadadi a L. Fan, „Experimental and computational study of constrained melting of phase change materials (PCM) inside a spherical capsule," *International Journal of Heat and Mass Transfer,* pp. 3464-3472, 2009.

[45] M. Paya-Marin, J. Lim, J.-F. Chen a R. Lawson, „Large scale test of a novel back-pass non-perforated unglazed solar air collector," *Renewable Energy,* pp. 871-880, 2015.

# ABSTRACT

The habilitation thesis deals with latent heat thermal energy storage (LHTES) in solar air heating. Solar radiation that used to be considered an alternative source of energy is becoming one of the mainstream energy sources with application in many areas from domestic hot water heating to industrial-scale power generation. The investigations of latent heat thermal energy storage in solar air heating reported in the thesis focused on two cases. The first case was LHTES integrated with the solar absorber plate of an air solar collector (solar air heater). Two experimental front-and-back pass air solar collectors were built. One collector comprised a light-weight solar absorber plate made of sheet metal. The solar absorber plate of the other collector consisted of 9 aluminum containers (CSM panels) filled with a paraffin-based PCM with the melting temperature of 42 °C. The performance of the collectors was investigated experimentally in the outdoor environment and in a climatic chamber. LHTES integrated with the solar absorber plate attenuated the outlet air temperature fluctuations under varying solar radiation intensity at the expense of lower thermal efficiency of the collector under steady-state conditions. A simulation model of the experimental air solar collectors was created in the TRNSYS simulation tool. An in-house TRNSYS type for modelling of heat transfer in phase change materials was used in the model. The experimental and numerical results were in good agreement.

The second case of LHTES reported in the thesis was a thermal storage unit for short-term heat storage in solar air heating. The investigated lab-scale LHTES unit contained 100 CSM panels filled with a paraffin-based PCM (the same type of CSM panels as in case of the solar air collector). The overall heat storage capacity of the panels, including the aluminum containers, was 3.3 kWh in the temperature range between 25 °C and 55 °C. The experiments were carried out in a lab environment. An electric air heater was used as a heat source, instead of an air solar collector. The experiments were carried out with almost constant inlet air temperature. The same airflow direction was used in both the heat storage and the heat release period. A 1D simulation model of the LHTES unit was developed for the numerical investigations in the TRNSYS simulation tool. The experimental and numerical results showed relatively good agreement though some discrepancies occurred when the PCM underwent melting or congealing. The developed numerical model was used for a parametric study of the thermal behavior of the LHTES unit as the unit is also applicable in other thermal energy systems with air as a heat transfer fluid (e.g. air-to-air heat pumps).



**Acknowledgement**

The author wishes to thank the following people for their invaluable contribution to this thesis:

doc. Ing. Milan Ostrý, Ph.D. for his help and advice with the thermal energy storage experiments.

Ing. Lubomír Klimeš, Ph.D. for his help with the numerical simulation of heat transfer in phase change materials.

Ing. Ondřej Pech and Ing. Jiří Hejčík, Ph.D. for their help with the air solar collector experiments.